SGI-R-81-052

INVERSION FOR t*(f)

G.M. LUNDQUIST

I.R. SAMOWITZ

SEMI-ANNUAL TECHNICAL REPORT

FOR PERIOD ENDING NOVEMBER 30, 1981

SPONSORED BY

DEFENSE ADVANCED RESEARCH PROJECTS AGENCY (DoD)

ARPA ORDER No. 3291-40

MONITORED BY AFOSR UNDER CONTRACT #F49620-81-C-0025

November 30, 1981

SIERRA GEOPHYSICS

15446 BELL-RED ROAD, SUITE 400 • REDMOND, WASHINGTON 98052 • (206) 881-8833

ARPA Order No. 3291-40

Program Code: 1A10

Effective date of Contract: November 1, 1980

Contract Expiration Date: October 31, 1982

Amount of Contract: $567,447

Principal Investigators and Phone No.:

Dr. G. M. Lundquist

Dr. D. M. Hadley

(206) 881-8833

Program Manager and Phone No.:

Mr. William J. Best

(202) 767-4908

Unclassified

SECURITY CLASSIFICATION OF THIS PAGE (When Data Entered)

REPORT DOCUMENTATION PAGE		READ INSTRUCTIONS BEFORE COMPLETING FORM
1. REPORT NUMBER AFOSR-TR- 81-0888	2. GOVT ACCESSION NO. AD-A110 308	3. RECIPIENT'S CATALOG NUMBER
4. TITLE (and Subtitle) INVERSION FOR T (*) (F)		5. TYPE OF REPORT & PERIOD COVERED Interim ~~12/1/80~~ 9/30/81
		6. PERFORMING ORG. REPORT NUMBER SGI-R-81-052
7. AUTHOR(s) G.M. Lundquist I.R. Samowitz		8. CONTRACT OR GRANT NUMBER(s) F49620-81-C-0025
9. PERFORMING ORGANIZATION NAME AND ADDRESS Sierra Geophysics, Inc. 15446 Bell-Red Rd., Suite 400 Redmond, WA 98052		10. PROGRAM ELEMENT, PROJECT, TASK AREA & WORK UNIT NUMBERS 61102F 2309/A1
11. CONTROLLING OFFICE NAME AND ADDRESS AFOSR/NP Bolling AFB, Bldg. #410 Wash DC 20332		12. REPORT DATE November 30, 1981 13. NUMBER OF PAGES
14. MONITORING AGENCY NAME & ADDRESS(if different from Controlling Office)		15. SECURITY CLASS. (of this report) Unclassified 15a. DECLASSIFICATION/DOWNGRADING SCHEDULE

16. DISTRIBUTION STATEMENT (of this Report)

Approved for public release, distribution unlimited

17. DISTRIBUTION STATEMENT (of the abstract entered in Block 20, if different from Report)

18. SUPPLEMENTARY NOTES

19. KEY WORDS (Continue on reverse side if necessary and identify by block number)

Q	receiver functions	Eastern Kazakh
t*	body waves	inversion
	NTS	

20. ABSTRACT (Continue on reverse side if necessary and identify by block number)

This technical report summarizes work done during the period December 1, 1980 thorugh September 30, 1981 based upon software developed and experience gained in modeling several forms of the Q filter. This report concentrates on the inversion theory to model the Q filter and to estimate the models of each parameter. Two spectral ratio data sets are used, PP/P and receiver function rates. The PP/P data set was limited to long period data and results indicate the necessity of using broader bandwidth data.

DD FORM 1 JAN 73 1473

Unclassified

SECURITY CLASSIFICATION OF THIS PAGE (When Data Entered)

The short period receiver function spectral ratios lead to consistent values of ∂t^* for several paths about the Eastern Kazakh and NTS test sites.

TABLE OF CONTENTS

LIST OF TABLES

LIST OF FIGURES

LIST OF FIGURES (Cont.)

EXECUTIVE SUMMARY

Of the earth filters that determine seismic waveforms, the Q filter is probably the least well constrained. Though anelastic attenuation reduces signal amplitude by several orders of magnitude at 5 Hz, the form of the Q filter is still in question. In this study, a form is adopted for Q(f) which meets the constraints of both microphysics and continuum mechanics. This is turn leads to the definition of t*(f) in terms of $\bar{\tau}_2$, a path averaged absorption band parameter. With the completion of the forward problem, an inverse theory is completed with the capability to model several forms of the Q filter and to estimate parameters of each model.

The inverse process is applied to two spectral ratio data sets, PP/P and receiver function ratios. The PP/P data were strictly long period, so only the difference, δt^*, in low frequency t* values could be estimated. In practice, the Q filter signal is masked by noise on the spectrum due to the crustal transfer function at the PP bounce point. The inverse method is demonstrated, but adequate estimates of attenuation properties will require broadband seismic data.

The receiver function spectral ratios are short period and thus provide much better resolution on Q. Consistent values of δt^* are found for several paths about the Eastern Kazakh and NTS nuclear test sites. In tests of model definition, the frequency dependent t^* models are shown to be

significantly better at fitting high frequency data than the constant Q (or constant t^*) assumption. Bandwidth and instrumental gain problems again prevent any absolute conclusions.

1. INTRODUCTION

The anelastic attenuation of a seismic wave can be written in terms of t^*, the weighted average of Q^{-1} over the seismic raypath. But, because t^* is a path property, estimation of t^* requires separation of anelastic effects from source and geometric properties. Spectral ratios have been very successful in such separation, using the ratio of seismogram at one receiver to that at another or the ratio of two phases at the same receiver to estimate δt^*, the difference in t^* for the two paths. Typically t^* is assumed to be independent of frequency, and δt^* is estimated from a linear fit to the graph of log spectral ratio-vs-frequency.

Strong evidence exists, however, that Q and therefore t^* must be frequency dependent (Lundquist and Cormier, 1980; Lundquist et al, 1980), and that the fit of a straight line is therefore not appropriate. This report will discuss the choice of a model for frequency dependent t^* and will develop the framework for inverting for t^* without the restrictive assumption of frequency independence. The inversion technique will then be tested against two different types of spectral ratios.

II. THEORY

The development of an inverse theory for frequency dependent t^* requires three steps. First, the foreward problem must be solved for seismic raypaths in general. Second, the specific spectral ratios under consideration must be examined and understood in detail. Finally, the inverse theory must be cast in terms of the relative behavior of parameters in the foreward problem. Each of these steps will be discussed in a separate section.

2.1 Q (f)

Q models may be constrained *a priori* to certain classes of frequency dependence and certain forms of depth dependence (Lundquist, 1979). An examination of anelasticity from both the continuum and microphysics points of view shows that all of the important physical dissipation mechanisms have two characteristics in common (Jackson and Anderson, 1970). They are all thermally activated processes, and they are all relaxation processes. Thus a general form may be written for the frequency dependency of a single mechanism without adopting any particular mechanism for attenuation in the earth. The Q^{-1} of this standard anelastic solid is a peaked function of frequency about $\omega = 1/\tau$, where τ is the relaxation time.

A distribution of such mechanisms may be assumed to exist in a complex solid such as the earth, giving attenuation over a broad range of frequencies. Liu et al

(1976) adopted the distribution in terms of relaxation time given by Gurevich (1964):

$$D(\tau) = \begin{cases} 1/\tau, & \tau_1 < \tau < \tau_2 \text{ sec/rad} \\ 0, & \text{otherwise} \end{cases} \qquad (1)$$

This defines an absorption band, as shown in Figure 1, where τ_1, and τ_2 are the half amplitude points at low and high frequencies, respectively. An absorption band rheology is clearly only a first approximation to the true frequency dependence of Q, but it is the simplest Q (f) model compatible with the microphysics of dissipation mechanisms.

The significance of activated process theory for Q(f,r) is that the theoretical depth dependence of relaxation time is an exponential function of pressure and inverse temperature. Essentially, τ increases rapidly with depth through the range of the asthenosphere, where increasing temperature dominates. Then τ decreases slowly as pressure effects dominate. The result is that the absorption band for a given mechanism must shift to high frequency over the asthenosphere and then to lower frequency with increasing depth. If the same mechanism is not active at all depths, then the picture becomes much more complex.

The conclusion, then, is that although the assumption that Q^{-1} may be modeled by an absorption band is valid on a pointwise basis, it is only approximately correct on a pathwise basis. The assumption of constant τ_2 is the same as saying that Q^{-1} (3Hz), say, is the same fraction of Q_m^{-1} at

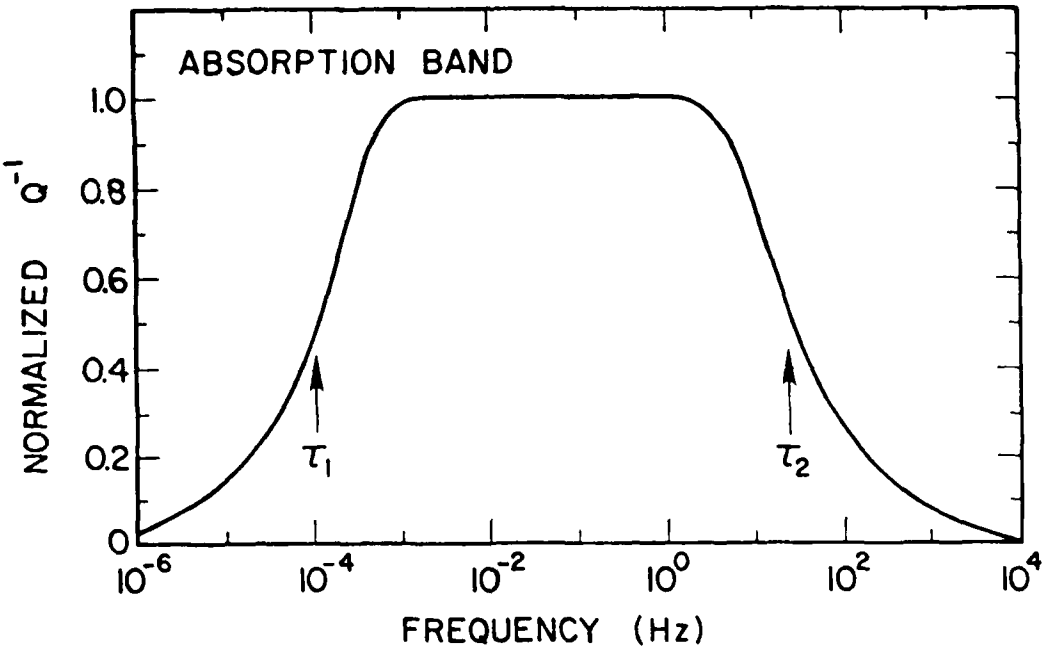

Figure 1. Normalized absorption band versus frequency; τ_1 and τ_2 are relaxation times at the low- and high- frequency half-amplitude points, respectively.

all depths. Because a seismogram is a path average, then any estimate of τ_2 measured from seismogram spectral ratios is a weighted average of τ_2 over the path. All values of τ_2 reported in this paper will have this restricted definition.

t^* is a path property which depends upon a weighted average of Q^{-1} over the path. The adoption of an absorption band model for a uniform medium leads to the definition.

$$t^*(\omega) = t^*_m \frac{2}{\pi} \tan^{-1} \left[\frac{\omega(\tau_1 - \tau_2)}{1+\omega^2 \tau_1 \tau_2} \right] \qquad (2)$$

which reduces to

$$t^*(\omega) \cong t^*_m \frac{2}{\pi} \tan^{-1} \left(\frac{1}{\omega \tau_2} \right) \qquad (3)$$

under the assumption that $\tau_1 >> \tau_2$. t^*_m is the t^* at the maximum of the absorption band, corresponding to t^* values reported in the literature for low frequencies. The path Q filter is given in terms of t^* by

$$\ln|F_Q| = -\pi f \, t^*_m \frac{2}{\pi} \tan^{-1} \left(\frac{1}{\omega \tau_2} \right) \qquad (4)$$

where f is frequency.

The spectral ratio of two seismograms can be defined in terms of equation (4) by

$$\log \frac{S_k}{S_o} = -2fB \left[t^*_{mk} \tan^{-1}\left(\frac{1}{\omega\tau_{2k}}\right) - t^*_{m0} \tan^{-1}\left(\frac{1}{\omega\tau_{20}}\right)\right] + C \quad (5)$$

where C is a relative gain factor. The spectral ratio is defined in terms of five parameters: t^*_{m0}, τ_{20}, t^*_{mk}, τ_{2k}, and C. Since the ratio is determined at many frequencies, the inverse problem becomes a least squares process. Equation (5) will be the basis for the inverse theory presented here.

Figures 2 and 3 show several examples of theoretical Q filters, corresponding to equation (4), and synthetic spectral ratios as defined by equation (5). A feature of Q filters defined by a frequency dependent t^* is that the amplitude spectrum on a log-log plot has two inflections, one determined by t^* and one by τ_2. For τ_2, greater than zero, the filter approaches a constant spectral level at high frequencies, in direct contrast to the frequency independent filters which fall exponentially at high frequency. This difference can amount to orders of magnitude difference in predicted spectral amplitudes, and will be significant in determining whether τ_2 is a required parameter in the Q filter.

2.2 Spectral Ratios

Two specific spectral ratio types will be discussed and tested in this report. The ratio of PP waves to the direct P arrival produces a δt^* which is a direct estimate of the t^* at the bounce point. The high quality spectral ratios

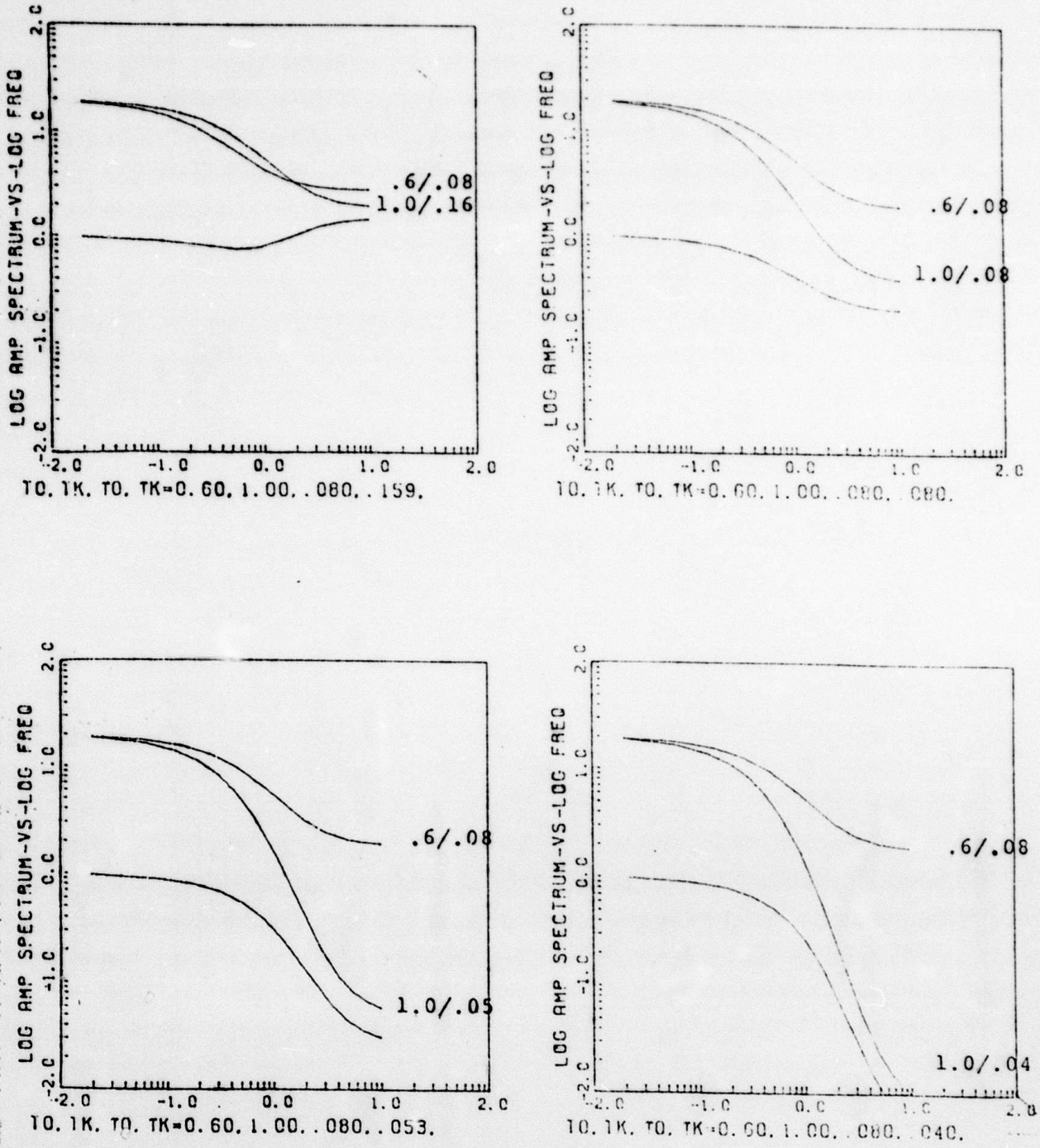

Figure 2. Examples of theoretical Q filters and synthetic spectral ratios.

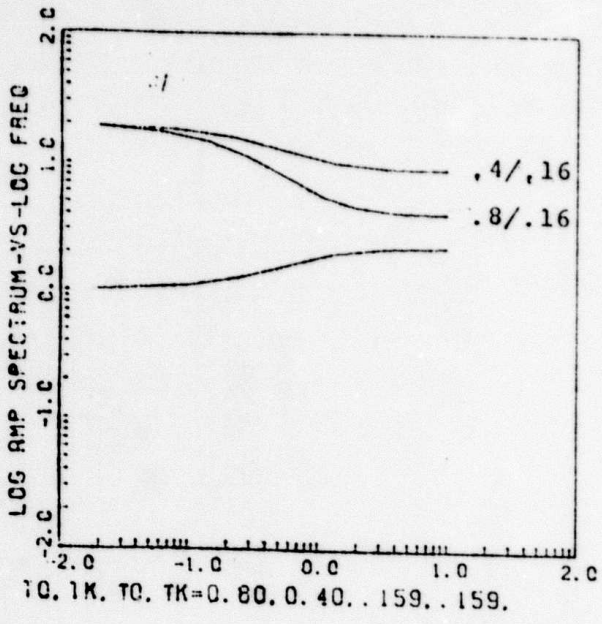

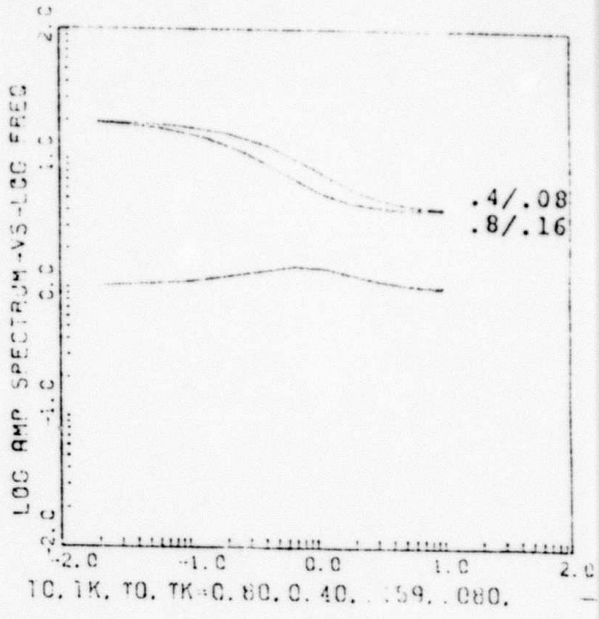

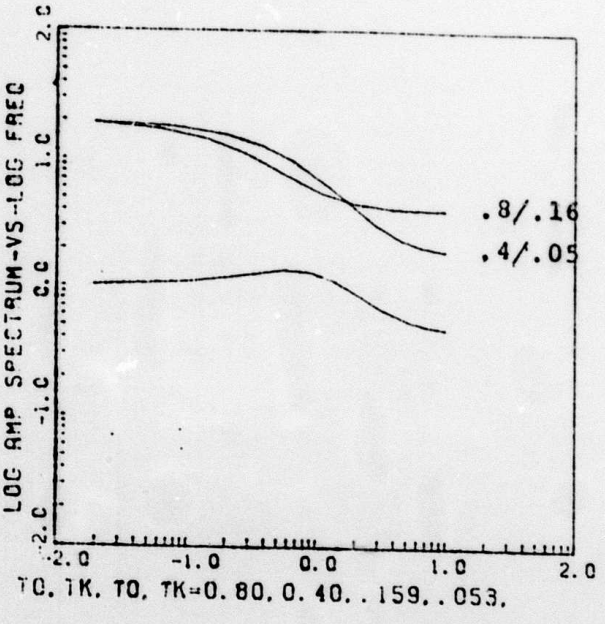

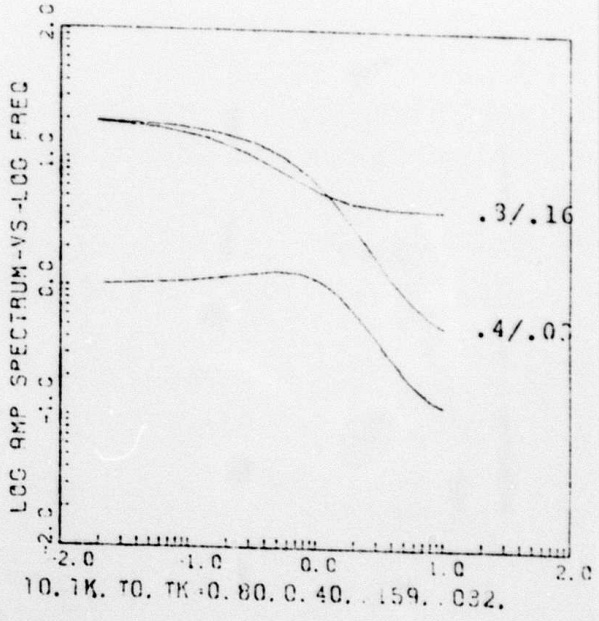

Figure 3. Examples of theoretical Q filters and synthetic spectral ratios.

defined during estimation of relative receiver functions (Lundquist et al, 1980) produce δt^* which represents the difference in anelastic attenuation between the two seismic raypaths. These ratios use the approximately symmetric nuclear explosion sources, and several estimates of the ratio are averaged to minimize contamination by source asymmetries.

A P wave seismogram trace may be defined by

$$S_p(t) = F(t) * C_s * G_p * Q_p * C_R * I \qquad (6)$$

where F is the source function; C_s and C_r are crustal transfer functions at source and receiver, respectively; G_p is the geometric attentuation; I is the instrument, and Q_p is the desired Q filter. The corresponding PP wave is

$$S_{pp}(t) = H\{F(t)\} * C_s * G_{pp} * Q_{pp} * C_B * C_B * D_{pp} * C_R * I \qquad (7)$$

where H implies Hilbert transform; C_B is the crustal transfer function at the bounce point, and D is the surface reflection coefficient. The Hilbert transform affects only the phase and is necessary for synthesis of PP from P, but it is not a necessary correction for spectral ratios.

The spectral ratio then is

$$R(\omega) = \frac{S_{pp(\omega)}}{S_p(\omega)} = \frac{G_{pp} \cdot D_{pp}}{G_p} \cdot \frac{Q_{pp} \cdot C_B \cdot C_B}{Q_p} \qquad (8)$$

Here the factors have been grouped to isolate the frequency independent quantities G and D from those with frequency dependence. The assumption that the source factors divide out is a statement that take-off angles do not vary significantly between P and PP rays. For shallow focus and distances of 80° and 40°, this implies an assumption that the source and source crustal response do not change over about 10° change in emergence angle. Violation of this assumption will be seen as a noise factor (or variance) in the spectral ratio.

In terms of log amplitude spectra,

$$|R(f)| = -\pi f B \left(t^*_{pp} - t^*_{p} \right) + \log\left(\frac{G_{pp} D_{pp}}{G_p} \right) + 2B \log C_B(f) \quad (9)$$

Equation (9) defines the basic data set and foreward solution for P/PP spectral ratios. The correspondence with equation (5) is clear, except that a noise term has now been added in terms of the frequency dependent bounce point crustal response. In practice, the spectral ratio will be smoothed by a running average to minimize the effects of C_B. That is, the Q filter is expected to cause the broad frequency dependence in the spectral ratio, while the crustal response is expected to cause a variance about the desired signal.

The δt^* determined by (9) may be interpreted as the t^* associated with the crust and upper mantle at the bounce

point, the only significant difference between the two travel paths. Note that

$$t^*_p = t^*_p(\Delta)$$

$$t^*_{pp} = 2\, t^*_p(\Delta/2)$$

But t^*_p has been observed to be nearly constant with distance, so

$$t^*_{pp} - t^*_p = t^*_p$$

which may be interpreted directly as a property of the bounce point. Indeed, this method may provide the only correct definition of t^* as a function of geographic location.

It is interesting to observe that each of the terms in (9) may eventually be recovered. The reflection coefficient and geometric spreading factors can be estimated from standard models, and any error will be recovered from the gain factor, C, in (5). This is true in the sense that the reflection coefficient is actually the zero frequency response of the crust. Since $C_B(\omega)$ may be assumed to have no broad frequency trends, then the ratio corrected for the estimated δt^* is a direct estimate of the amplitude spectrum of C_B.

As a final note on PP/P spectral ratios, an independent estimate of the quality of the δt^* values may be obtained from time domain synthesis of the PP waveform from the P waveform.

$$\hat{S}_{pp}(\omega) = H\left\{S_p(\omega)\right\} \cdot Q\left(\delta t^*\right) \cdot \frac{G_{pp}}{G_p} \cdot D_{pp} \qquad (10)$$

The error between the estimate, S_{pp} and the observed PP seismogram will result primarily from inability to model C_B, but the comparison of waveforms will be a verification of the assumptions made in this analysis. Poor time domain fits can also be an indication of the presence of uncorrelated high frequency noise, which is treated as signal by spectral ratio technique.

Receiver function spectral ratios differ from PP/P ratios in that seismograms from two separate stations are used in the ratio. Thus, no factors may be assumed a priori to divide out.

$$R(\omega) = \frac{S_i(\omega)}{S_o(\omega)} = \frac{G_i}{G_o} \cdot \frac{Q_i}{Q_o} \cdot \frac{C_{Ri}}{C_{Ro}} \cdot \frac{F_i}{F_o} \cdot \frac{C_{Si}}{C_{So}} \cdot \frac{I_i}{I_o} \qquad (11)$$

Here the factors have been grouped according to importance. The ratio of geometric spreading factors is a simple gain factor with no frequency dependence. The factors in the last bracket will divide out if the source is symmetric (an explosion), the source crustal layering is flat, and the instrument responses are known. Unfortunately, though the shape of the instrument response curves are known, gain factors often are not. Ideally, both G and I are known; so that C in (5) is zero. In practice, azimuthal and take-off

angle asymmetries exist in S and C_s, leaving uncancelled frequency dependent noise, $N(\omega)$, in the spectral ratio. But the asymmetries are dependent upon source location and source depth, so averaging over several sources confined to a limited region (an explosion test site) reduces the noise factor. This process produced clean relative receiver functions for stations about the Eastern Kazakh test site in Russia (Lundquist et al, 1980c), but was less successful for the more complex NTS in Nevada (Lundquist et al, 1981).

With these observations in mind, (11) can be reduced to

$$\log \left|R(f)\right| = -\pi f B(t_i^* - t_o^*) + B \log C + B \log \left|\frac{C_{Ri}}{C_{Ro}}\right| + N(f) \qquad (12)$$

where C includes geometric and instrumental gain factors. For Q inversion, the ratio of receiver crustal responses becomes the most important noise term, dominating the residual noise due to source effects. The variance due to these factors can to some extent be reduced by smoothing the spectral ratio, at which time equation (12) defines the data set and foreward problem for the receiver function spectral ratios.

2.3 The Inverse Problem

The inverse problem for a frequency dependent t* can be written as an error minimization problem with five unknowns in the presence of noise. This is true, under the

assumptions stated here, for a wide range of spectral ratio types. Thus an inverse program will be a useful tool for the analysis of path attenuation in a variety of circumstances.

Let the solution the the foreward problem define a vector

$$g(\omega) = c\ h\ (f,\ t_o^*,\ \tau_o,\ t_k^*,\ \tau_k) \qquad (13)$$

where c is the overall gain factor, and h implies function. Using the notation $g_i = g\ (f_i)$, the partial derivative matrix may be defined as:

$$A_{ij} = \frac{\partial g_i}{\partial m_j} \quad , m_j = C,\ t^*_1,\ \tau_1,\ t^*_2,\ \tau_2$$

Then an increment of change in the model parameters produces an increment of change in g according to

$$\delta g_i = A_{ij}\ \delta_{mj}$$

The observed spectral ratio, r_i, may be compared to the foreward problem solution to define an error vector

$$d_i \equiv r_i - g_i$$

The object of the inversion is to find a set of m_j such that

the RMS quantity

$$\left\| d_i - A_{ij}\ \delta m_j \right\|$$

is minimized. The solution for δm_j gives

$$\delta \hat{m}_j = (A^T A)^{-1}\ A^T\ d \tag{14}$$

where the $\hat{}$ implies estimate.

In the presence of noise

$$\delta \hat{m}_j = (A^T A + \sigma^2 I)^{-1}\ A^T\ d \tag{15}$$

where σ is the noise variance. If weights are added,

$$\delta \hat{m}_j = (A^T\ WA + \sigma^2 I)^{-1}\ A^T\ Wd \tag{16}$$

The partial derivatives are given by

$$\frac{\partial g_i}{\partial mj} = \frac{\partial}{\delta mj} \left\{ -2fB \left[t_k^* \tan^{-1}\left(\frac{1}{\omega_i \tau_k}\right) - t_o^* \tan^{-1} \left(\frac{1}{\omega_i \tau_o}\right)\right] + C \right\}$$

$$\frac{\partial g_i}{\partial t_o^*} = -2fB \left[- \tan^{-1} \frac{1}{\omega \tau_o} \right]$$

$$\frac{\partial g_i}{\partial \tau_o} = -2fB \left[\frac{t_o^* \omega_i}{1+\omega^2 \tau_o^2} \right]$$

$$\frac{\partial g_i}{\partial t_k^*} = -2fB \left[\tan^{-1} \frac{1}{\omega \tau k} \right]$$

$$\frac{\partial g_i}{\partial \tau_k} = -2fB \left[\frac{-t^* \omega_i}{1+\omega_i^2 \tau_k^2} \right]$$

$$\frac{\partial g_i}{\partial c} = 1$$

Figure 4 shows an inversion run on noise-free synthetic data. The computer caption underneath the figure provides the critical information on this run, including final values for the five variables, the starting values, weights, number of iterations and the error. The bandlimited data set used is representative of the widest frequency range likely to be realized in short-period spectral ratios of digital data. Bandlimiting severly reduces the resolution in the inverse, and is partially responsible for the error in the final values of model parameters.

Another source of error in these inversions is tradeoff, both between t^* and τ_2 and between the two t^*'s and C. Thus the starting values and judicious use of weights is critical to obtaining correct results. In the work to be presented in the next section, multiple tests, reduction of variables and solution for differences rather than absolute values will all be used to reduce the effects of tradeoff.

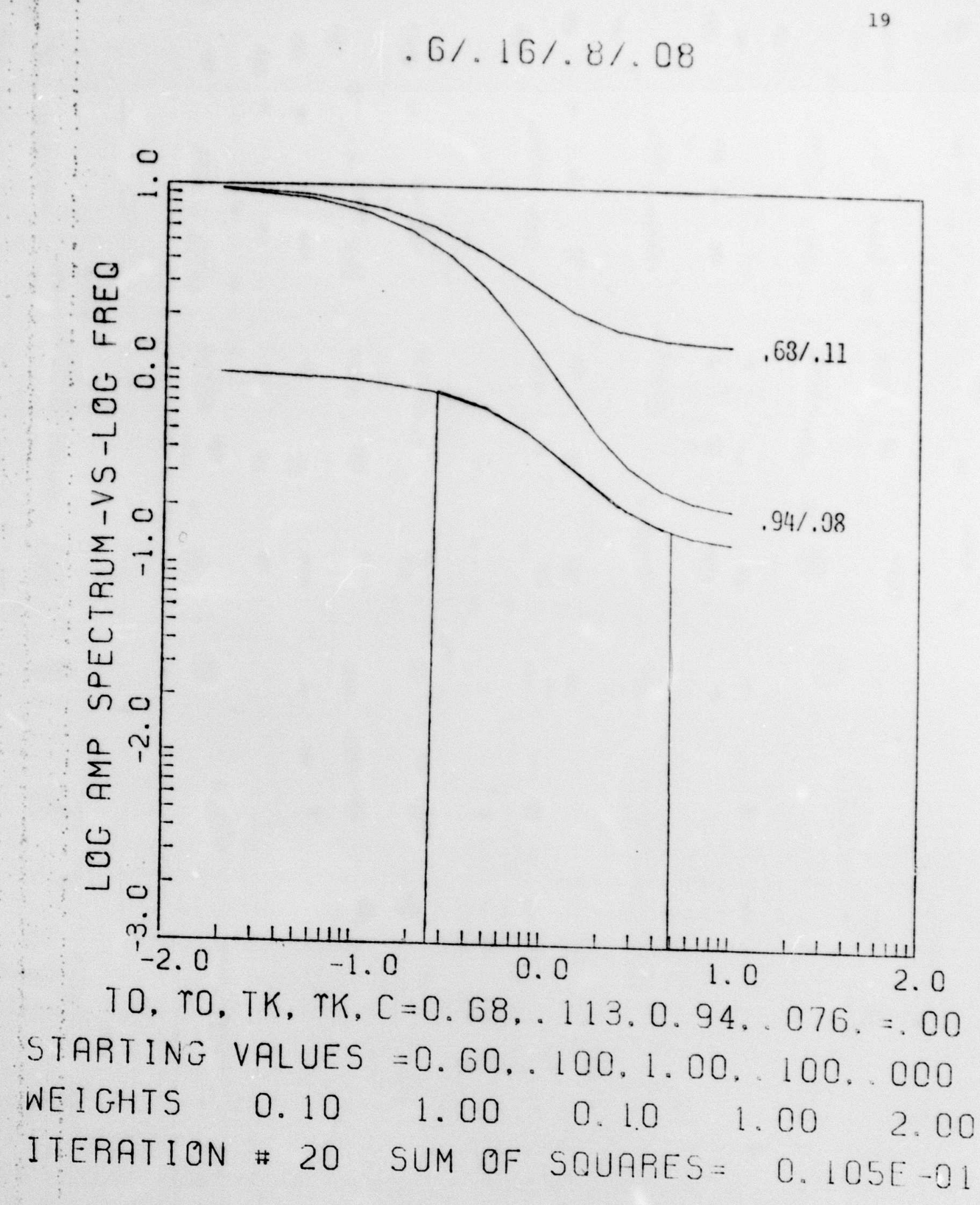

Figure 4. Results of t* inversion on noise-free synthetic data

III. DATA AND RESULTS

3.1 PP/P Spectral Ratios

The spectral ratio of PP/P waves may be interpreted in terms of anelastic properties in the crust and upper mantle of the bounce point. Two bounce points were chosen for study here, one at the Soviet nuclear test site in eastern Kazakhistan, and one in the east Pacific near the Hawaiian Islands. The first represents conditions of an old thick continental crust, while the second represents a young thin oceanic crust. A third bounce point at NTS representing a tectonic crust will be examined in a future report.

For each bounce point, source receiver pairs were sought which had distances in the range 60 to 85°. For the Soviet bounce point, sources in the Kuriles and Japan were recorded in the Mediteranean region and sources in southern Asia were recorded in Scandinavia. This provided a wide azimuthal coverage, as is shown in Figure 5, around a region of about 5° radius (550km) from the Russian nuclear test sites. The oceanic crust was studied using Tonga-Fiji earthquakes recorded at stations in the western U.S. These bounce points were constrained to be further than 2° from the Hawaiian Islands, so that the reflection would occur in simple crust. Table 1 lists the source/receiver pairs used in this study.

WWSSN data were used for this part of the study because of the relative rarity of paths to digital stations. Though short period records were sought, either the PP was below noise level or the P was off scale. Thus this analysis is

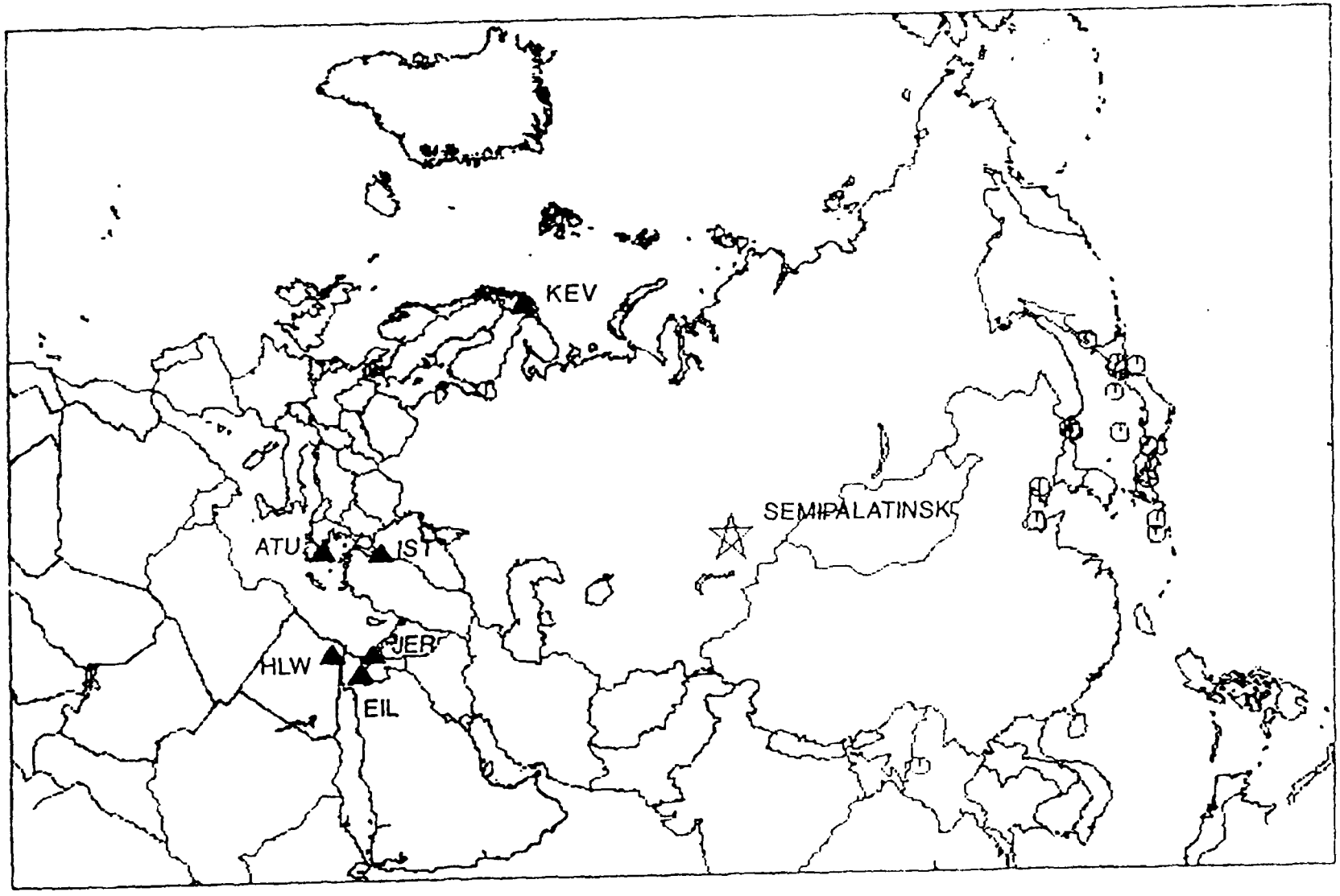

Figure 5. Azimuthal coverage of PP/P for Eastern Kazakh bounce point. The triangles represent WWSSN stations, the octagons represent the epicenters, and the star represents Semipalatinsk, the bounce point.

TABLE 1. Data set for PP/P t* inversion

KAZAKH BOUNCE POINT

REGION	DATE	DEPTH	Δ	STATION
Near E. Coast Honshu, Japan	3-16-65	34.00	85.41°	HLW
Ryukyu Islands	9-21-65	199.00	82.9°	ATU
So. Honshu, Japan	8-13-67	357.00	83.41°	ATU
Ryukyu Islands	5-14-68	162.00	83.16°	ATU
Shikoku, Japan	8-5-68	41.00	82.81°	ATU
Sea of Japan	3-31-69	417.00	81.43°	HLW
E. Russia-N.E. China Border	4-10-69	555.00	73.39° 77.18°	HLW JER
Northeastern China	7-18-69	33.00	66.48°	IST
Burma-India Border	10-17-69	134.00	60.88°	KEV
Sakhalin Island	12-18-69	344.00	80.13°	EIL
Eastern Sea of Japan	6-10-71	226.00	82.43°	HLW
E. Russia-N.E. China Border	9-10-73	532.00	74.75°	EIL
Hokkaido, Japan	11-8-74	130.00	83.75°	HLW
Northeastern China	2-4-75	33.00	67.14°	IST

PACIFIC OCEAN BOUNCE POINT

REGION	DATE	DEPTH	Δ	STATION
Fiji	1-26-72	668.00	77.10°	BKS
Fiji	5-9-72	568.00	76.74°	GSC
Fiji	12-19-73	246.00	79.51° 77.83°	COR GSC
Fiji	7-6-77	594.00	78.16°	BKS

limited to long period WWSSN seismograms. Each seismogram was digitized four times, and each digital copy was compared to the original to verify the accuracy. The four traces were then averaged, corrected for paper magnification, skew of the recording system and instrument gain factor.

The resulting spectral ratios had a useful bandwidth of one decade, from .05 to .5 Hz. Because the effects of anelasticity is small at low frequencies, and because τ_2 has been found to be a high frequency parameter (Lundquist and Cormier, 1979), the parameters in the PP/P inversions were reduced to t^*_p, t^*_{pp} and C, by setting τ_2 to zero and applying weights to keep it small. Without frequency dependence, there is total tradeoff between the t^* values, so the results of this experiment can only be interpreted in terms of δt^*_m, the low frequency difference in average path attenuation.

An example of a PP/P spectral ratio inversion is shown in Figure 6 for a Kurile source recorded at station EIL in Israel. Both time and frequency domain results are shown, and both waveform fitting and spectral fitting are compatible with $\delta t^* = 0.8$sec. The amplitude of the variance on the spectrum is small, implying a simple crust at the bounce point. The time domain results confirm this conclusion showing that the PP waveform is the theoretical Hilbert transform of the P wave.

Unfortunately, the success of Figure 6 is not typical. The range of scatter is given as a histogram in Figure 7,

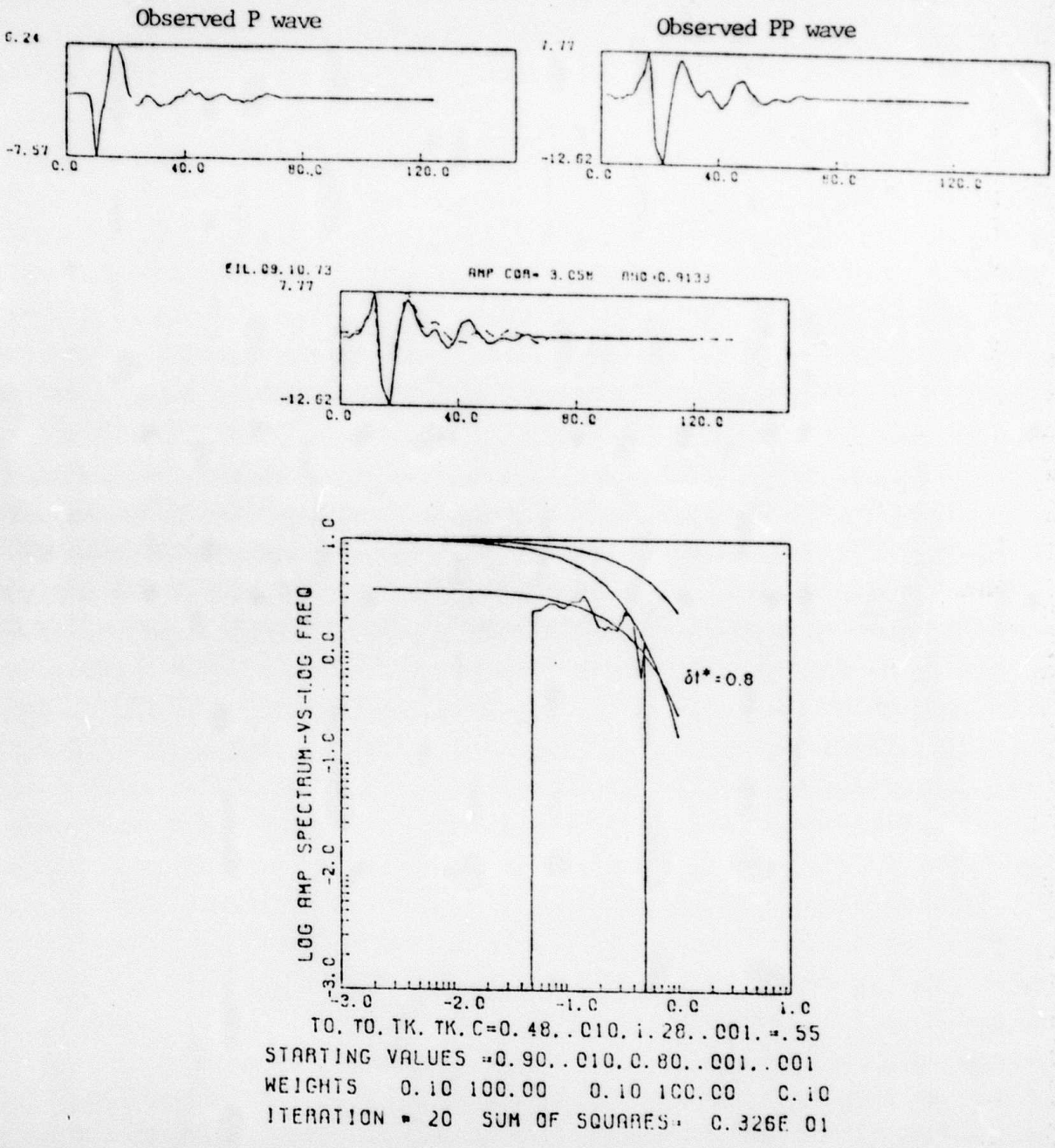

Figure 6. PP/P spectral ratio inversion for 9/10/73 recorded at station EIL with $\delta t^*=0.8$sec. For the waveform comparison, the observed PP wave is shown by the solid line, the synthetic PP is shown by the dashed line.

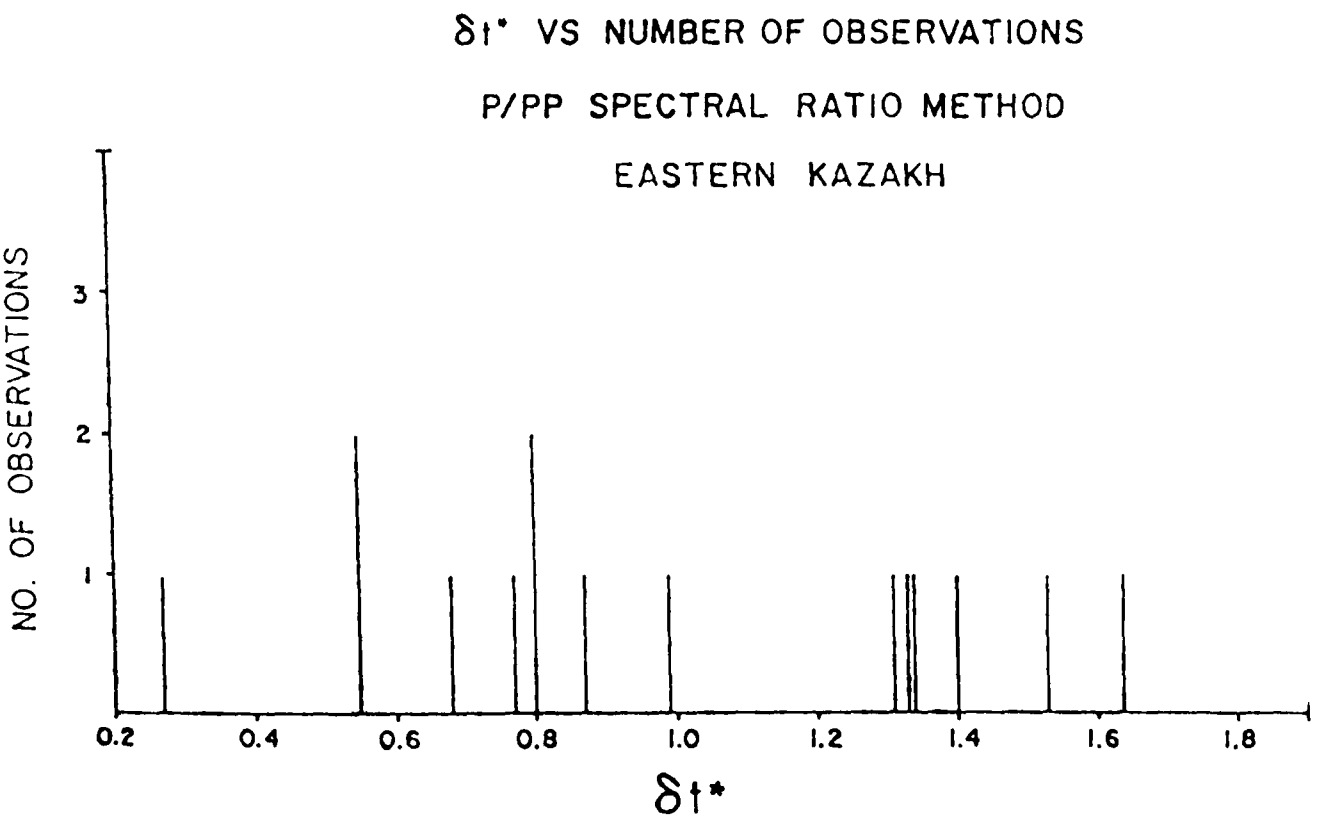

Figure 7. Histogram of δt^* inversion results for Eastern Kazakh bounce point.

and four additional examples are shown in Figures 8-11 with a range in δt^* of .27 to 1.4 sec. Examination of the spectra shows that each one has a much larger variance than that shown in Figure 6. The conclusion must be that the noise added to the spectrum at the crustal bounce point is commonly so great as to mask the anelastic attenuation seen by these low frequencies.

Two simple tests are shown in Figure 12 to demonstrate the level of signal sought by the PP/P inversion. The plot on the right shows theoretical spectra at δt^* values of .4 to 1.2 sec. For data bandlimited at .5 Hz., the maximum amplitude variation for a difference in δt^* of 0.8 is a factor of four, and most of the significant amplitude variation occurs in the range .3 to .5Hz. Thus noise at these frequencies can easily dominate the effects of anelasticity. The time domain test confirm that a change of .8 sec in δt^* has virtually no effect on the results. That is, there is no resolution in δt^* using long period time domain synthesis.

Similar results are observed for the Pacific Ocean bounce point, as is shown in Figures 13 and 14. These tests found that rather than being simpler, the oceanic bounce point produces a more complex waveform. The example in Figure 13 is one of the few cases where the PP is a simple Hilbert transform of the P wave. In addition, a number of PP waves were observed to have greater amplitude than the corresponding P wave, giving a negative δt^*. Such a con-

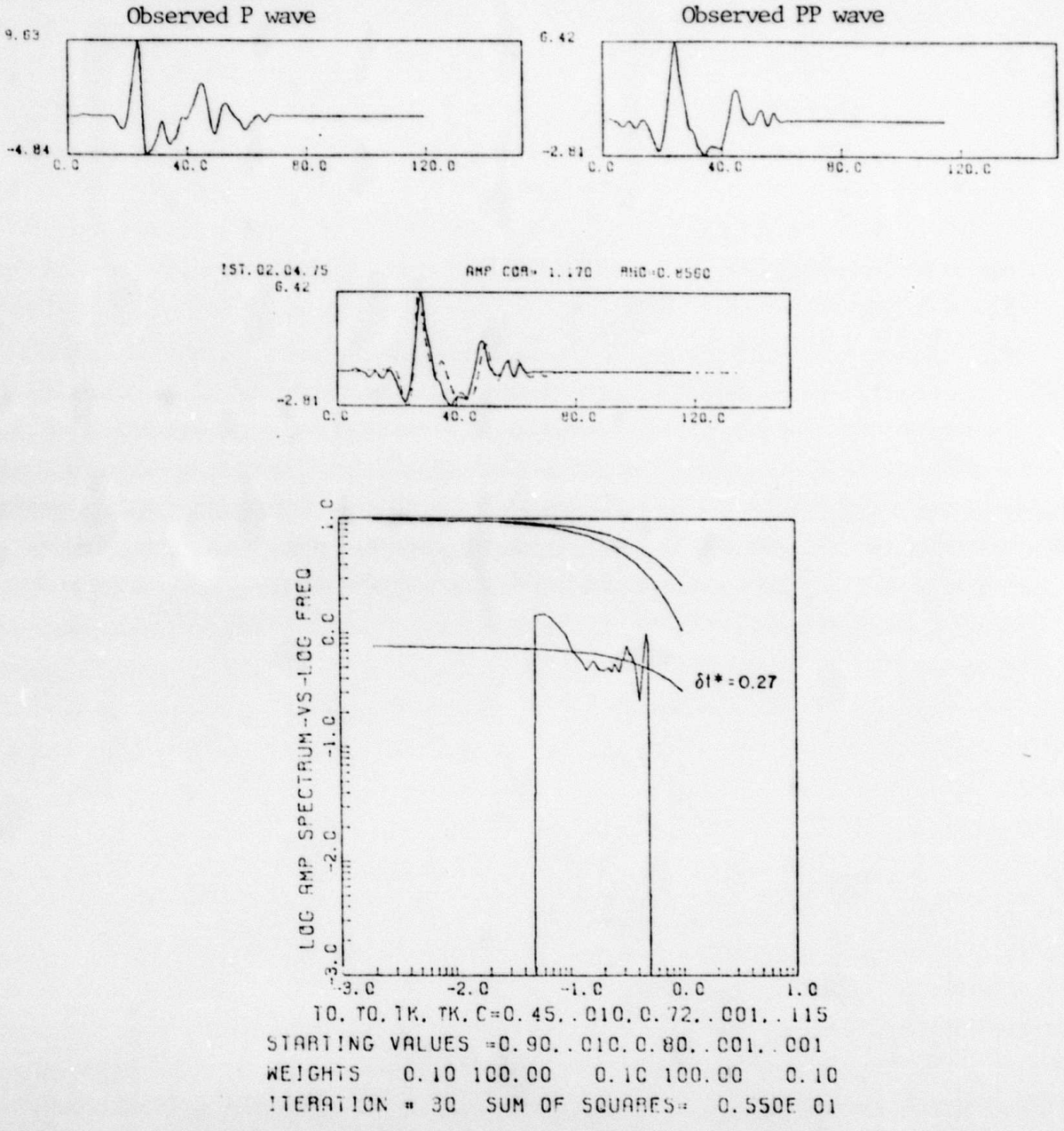

Figure 8. PP/P spectral ratio inversion for 2/4/75 recorded at station IST with $\delta t^*=0.27$sec. For the waveform comparison, the observed PP wave is shown by the solid line, the synthetic PP is shown by the dashed line.

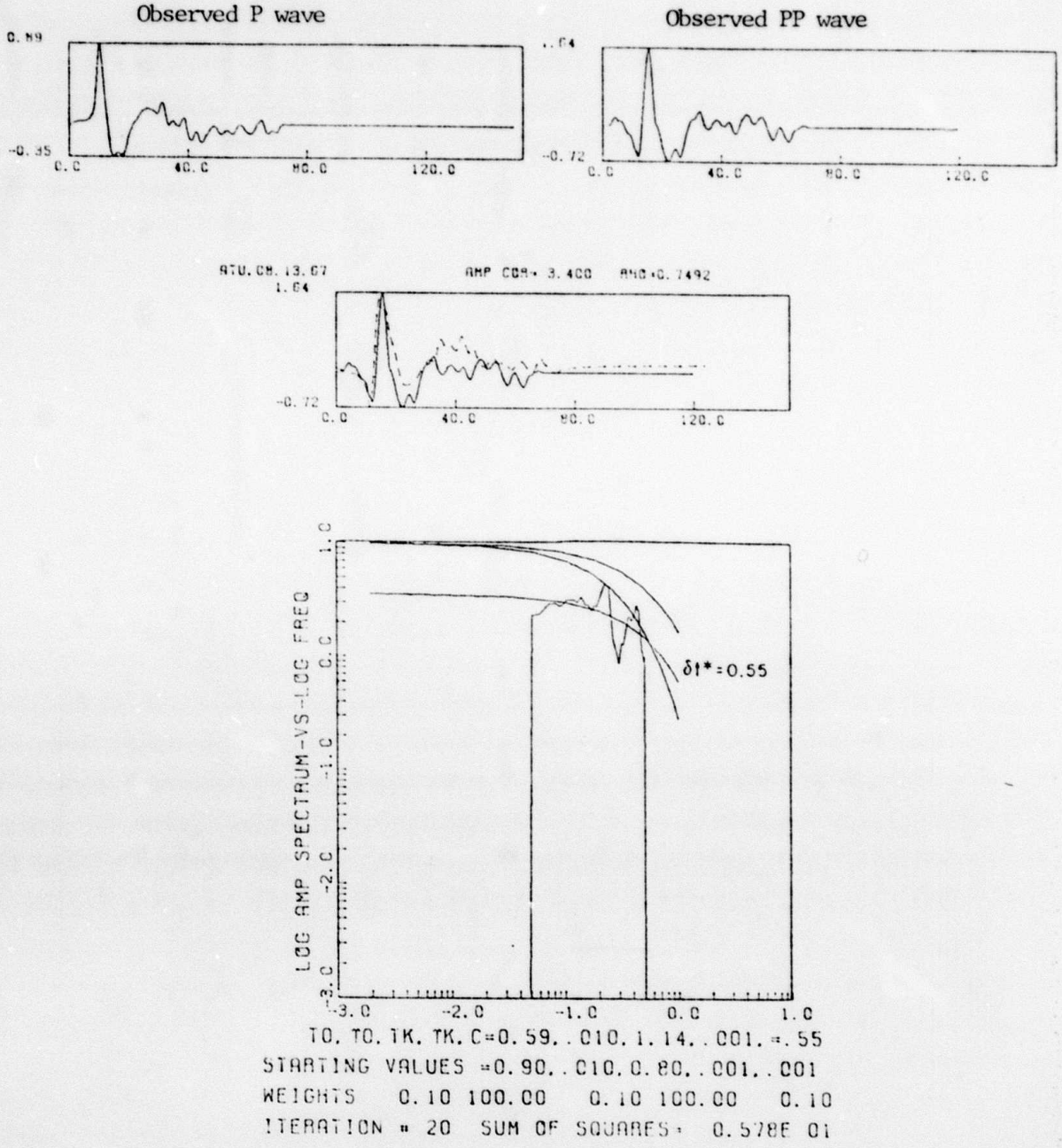

Figure 9. PP/P spectral ratio inversion for 8/13/67 recorded at station ATU with $\delta t^*=0.55$sec. For the waveform comparison, the observed PP wave is shown by the solid line, the synthetic PP is shown by the dashed line.

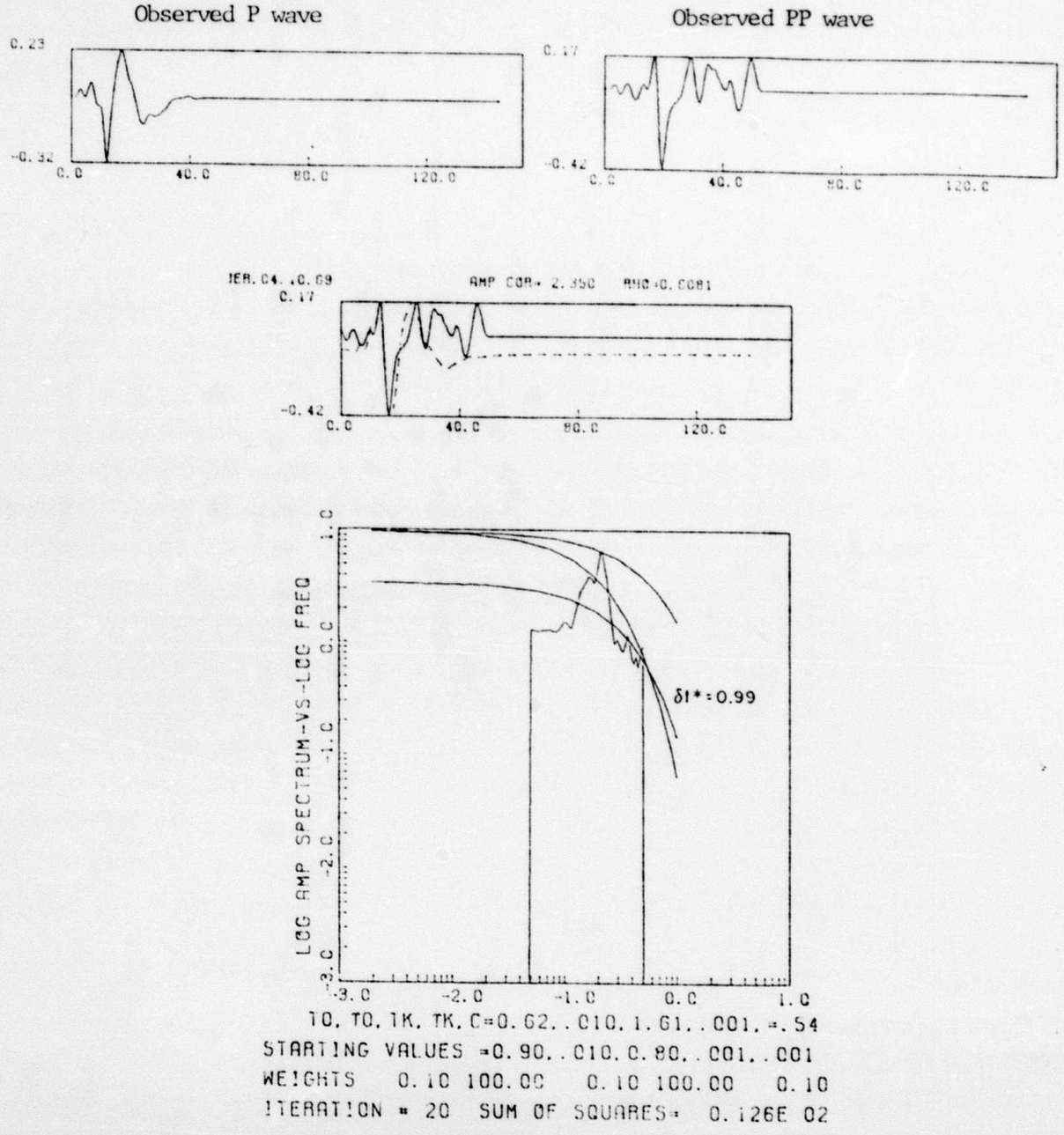

Figure 10. PP/P spectral ratio inversion for 4/10/69 recorded at station JER with $\delta t^*=0.99$sec. For the waveform comparison, the observed PP wave is shown by the solid line, the synthetic PP is shown by the dashed line.

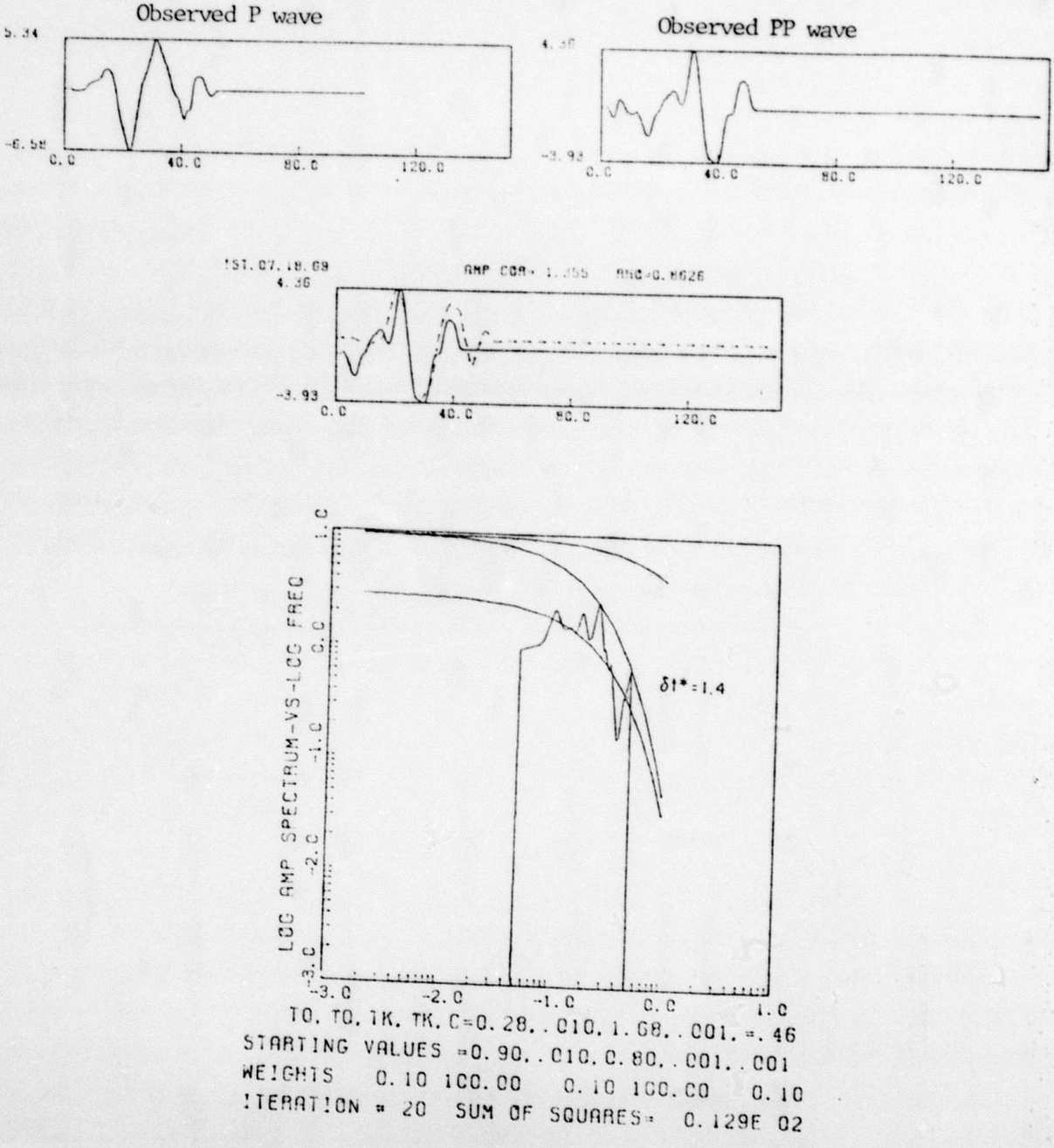

Figure 11. PP/P spectral ratio inversion for 7/18/69 recorded at station IST with δt^*=1.4sec. For the waveform comparison, the observed PP wave is shown by the solid line, the synthetic PP is shown by the dashed line.

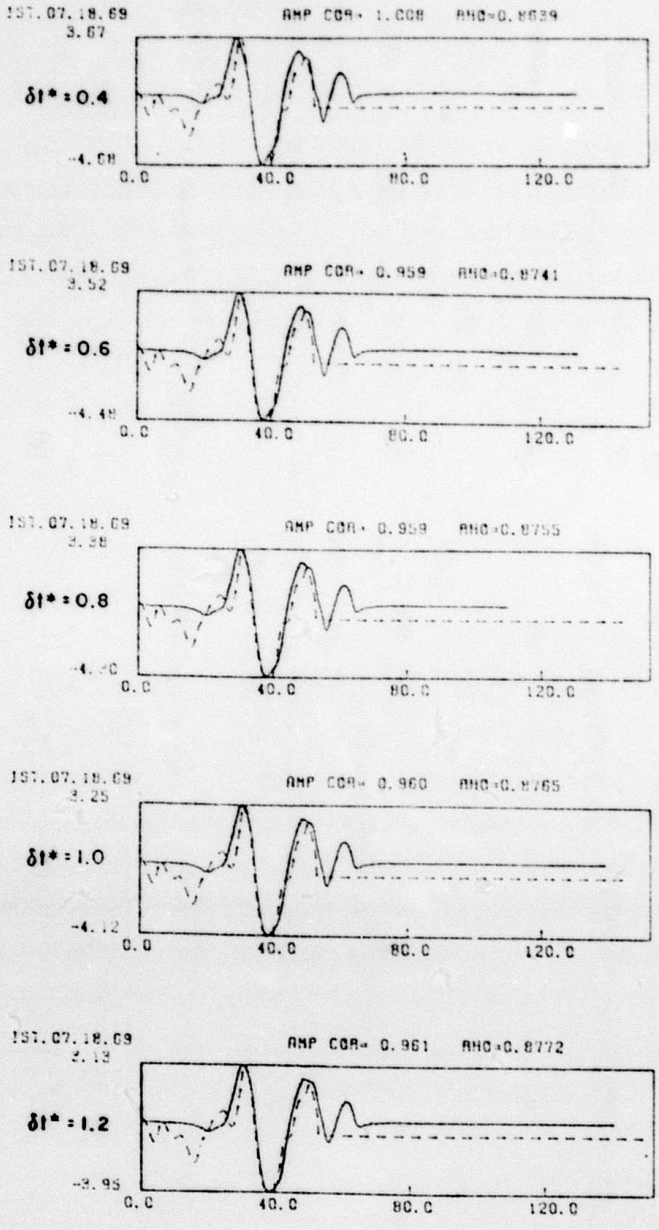

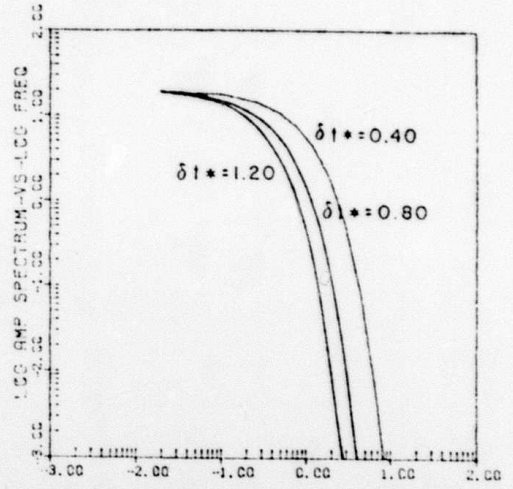

Figure 12. Test results are shown for synthetic seismograms and Q filters as a function of δt^*. The observed seismogram (dashed line) is compared with five different synthetic seismograms (solid line) computed with different δt^* values. Three different Q filters are compared to show their effect.

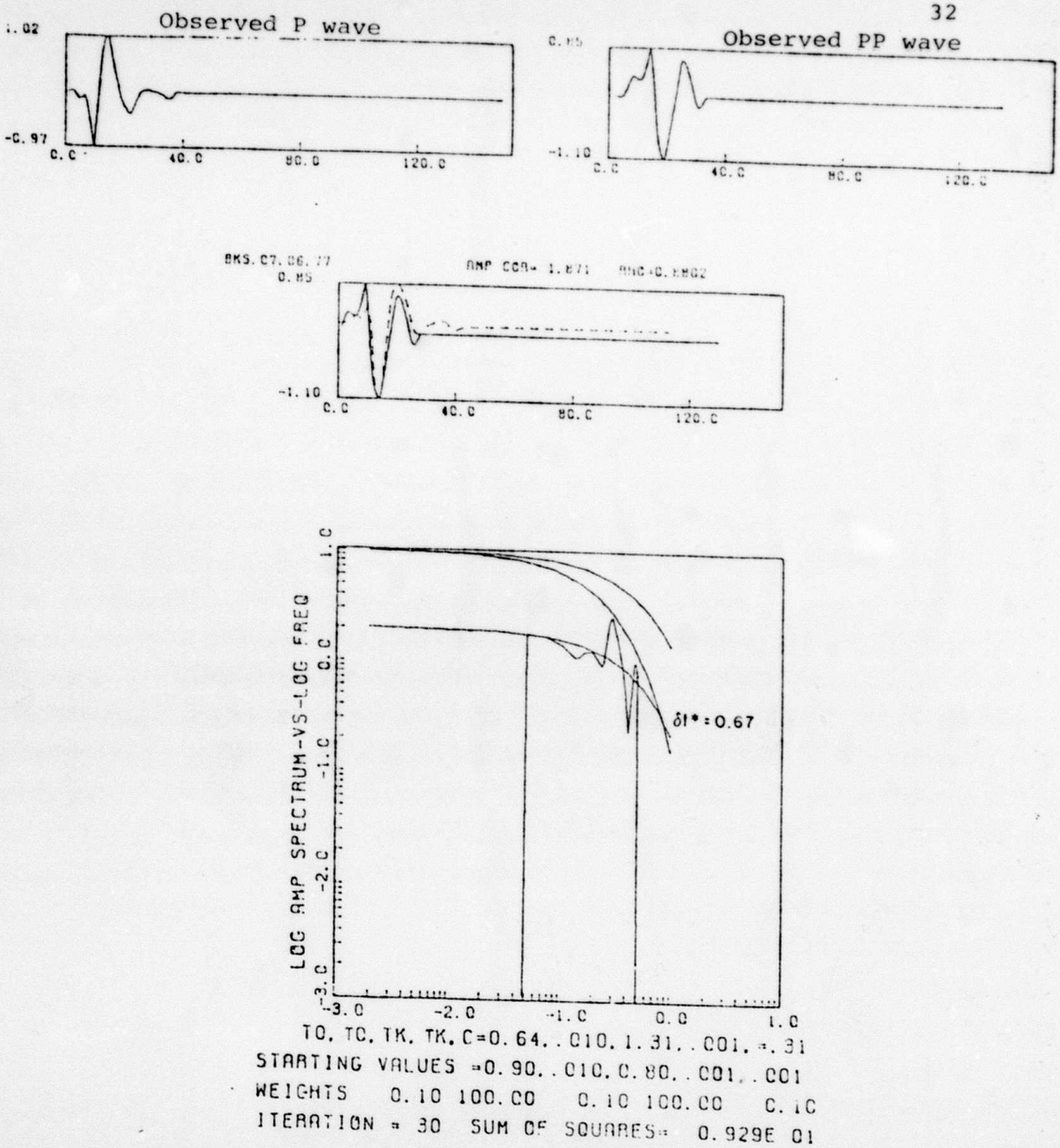

Figure 13. PP/P spectral ratio inversion for 7/6/77 recorded at station BKS with $\delta t^*=.67$. For the waveform comparison, the observed PP wave is shown by the solid line, the synthetic PP is shown by the dashed line.

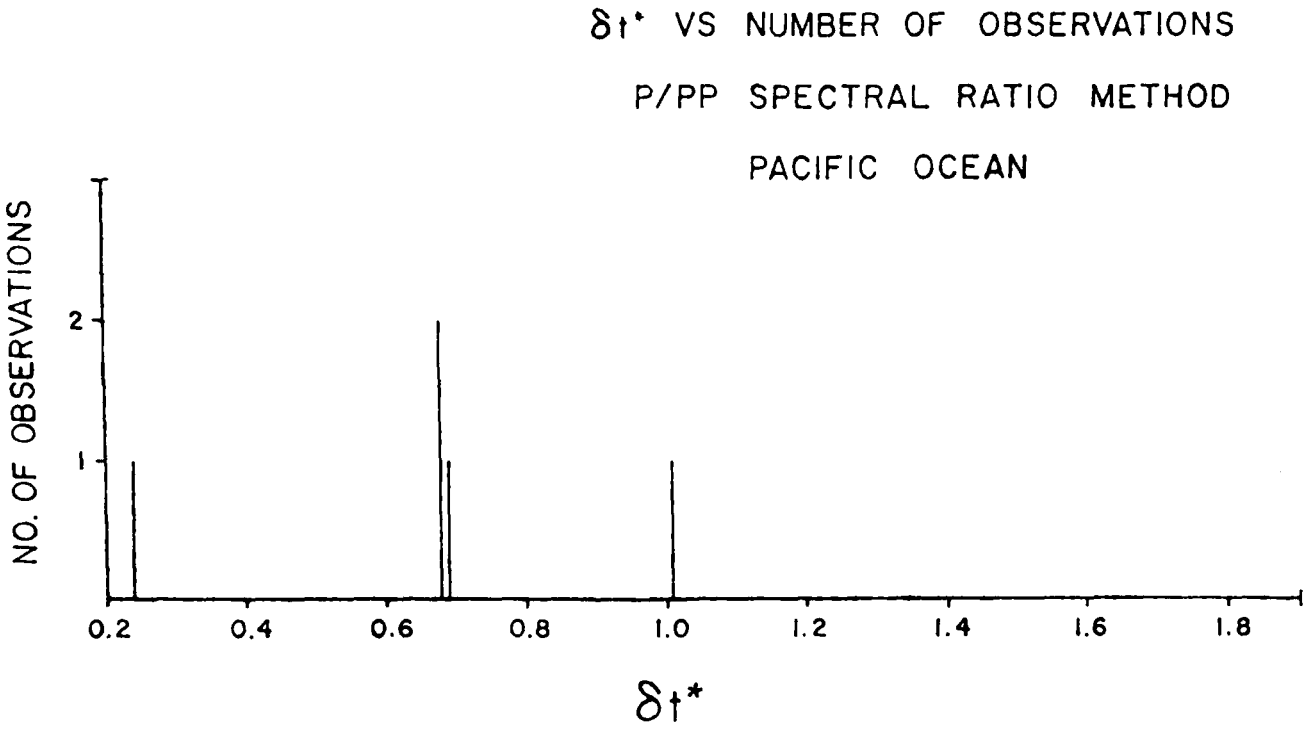

Figure 14. Histogram of δt* inversion results for Pacific Ocean bounce point.

dition requires a significant source anisotropy, such as takeoff angles near the nodal planes.

The conclusions to be reached from this early study of PP/P inversion for δt^* is that bandwidth is the greatest problem. There simply is not enough t^* signal in the low frequency crustal noise to permit clear estimation of t^*. Adequate results will be achieved only when short period or broadband data are brought to bear upon the problem. The method is, however, quite effective, and it will not be limited by assumptions of frequency independent t^* when high frequencies are added to the data set.

3.2 Receiver Function Spectral Ratios

Two data sets will be used in this section, representing studies of receiver functions for stations about the Eastern Kazakh Test Site and the Nevada Test Site. Table 2 lists the stations used and their distance and azimuth relation to the source regions.

An example of an inversion is shown in Figure 15 for the ratio of CHTO to Alice Springs, Australia (ASA) from an Eastern Kazakh source. In this case the reference path had parameters t^* = .63 sec and τ_2 = .15 sec; while the path to CHTO has a nearly frequency independent t^* = .21 sec. This particular spectral ratio has a great deal of character, and very similar results are found for a wide range of starting values and weights. But examination of the tradeoff matrix shows that only differences between the t^* or τ_2 values are tightly constrained.

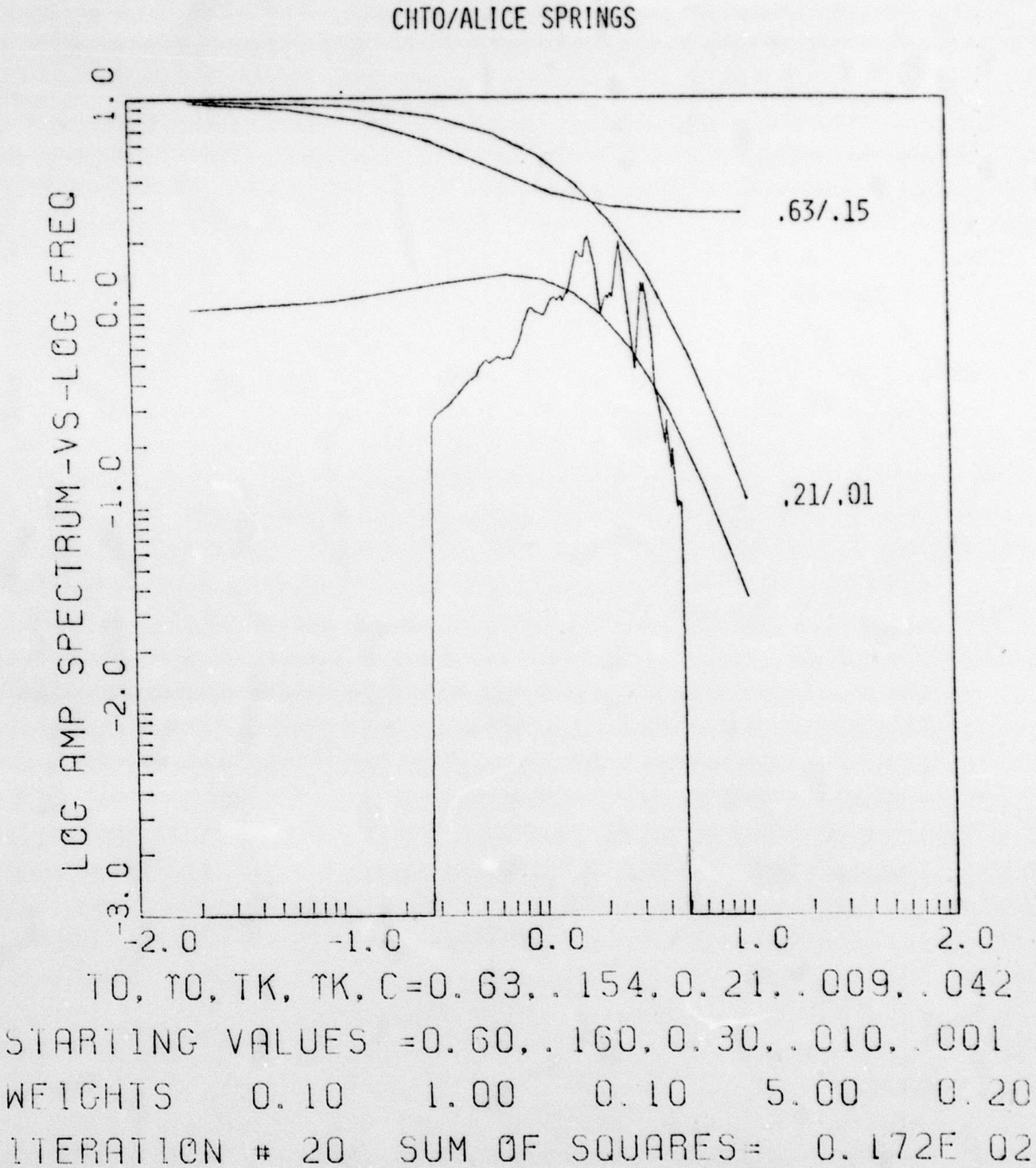

Figure 15. t* inversion on receiver function spectral ratio of CHTO to ASA for an Eastern Kazakh source.

Table 2. Station Set for t^* Inversion

Station	Δ	Azimuth
Eastern Kazakh Test Site		
Alice Springs (ASA)	88°	131°
ANMO	95°	4°
CHTO	35°	145°
KSRS	37°	90°
PINEDALE	83°	340°
Nevada Test Site		
BOCO	51°	119°
GRFO	82°	31°
KONO	74°	25°
KSRS	85°	314°
MAJO	79°	308°
NAO	73°	24°
ZOBO	70°	130°

In order to reduce the tradeoff problems, several spectral ratios may be put into one inversion. Using the same reference station for each ratio, an inversion on four ratios can be solved for the properties of five paths. In such a case the tradeoff between individual paths is minimal, leaving tradeoff between t^* and τ_2 for each path. In practice, if the spectral ratios have a great deal of character, few combinations exist which will satisfy a four ratio inversion.

Figures 16 and 17 show example of four ratio inversions for the two source regions using reference stations ASA and BOCO, respectively. Note that the values found for the CHTO ratio compare very well to those shown in Figure 15. Comparison may also be made between the two values for KSRS, the only station common to the two arrays. If the results are taken at face value, then the attenuation to KSRS from Nevada is slightly greater than from central Asia. In a difficult comparison, however, although the paths to KONO and NAO are very similar, the combination of δt^* and $\delta\tau_2$ show significantly different path attenuation from NTS.

The conclusion must be that the method shows promise, but that not all problems have been solved. Two separate classes of problem may be defined: inadequate or bandlimited data, and the intricacies of the inverse problem. The first problem must be solved by augmenting the current data sets, and the second problem may be approached by testing the procedure under a variety of conditions. A few such tests will now be discussed.

Q ASSUMED TO BE FREQUENCY DEPENDENT

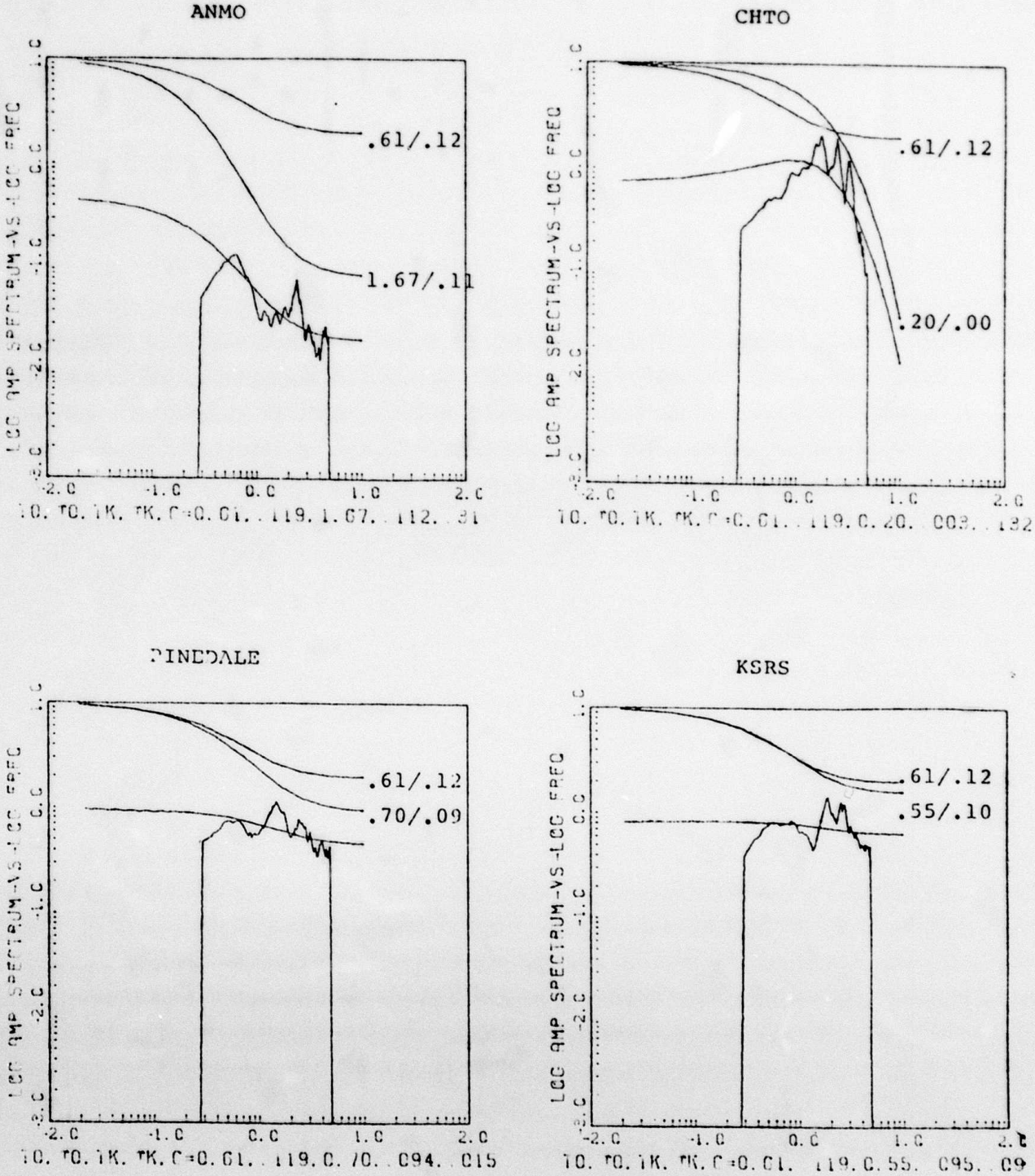

Figure 16. t* inversion on four receiver function spectral ratios using reference station ASA for Eastern Kazakh sources.

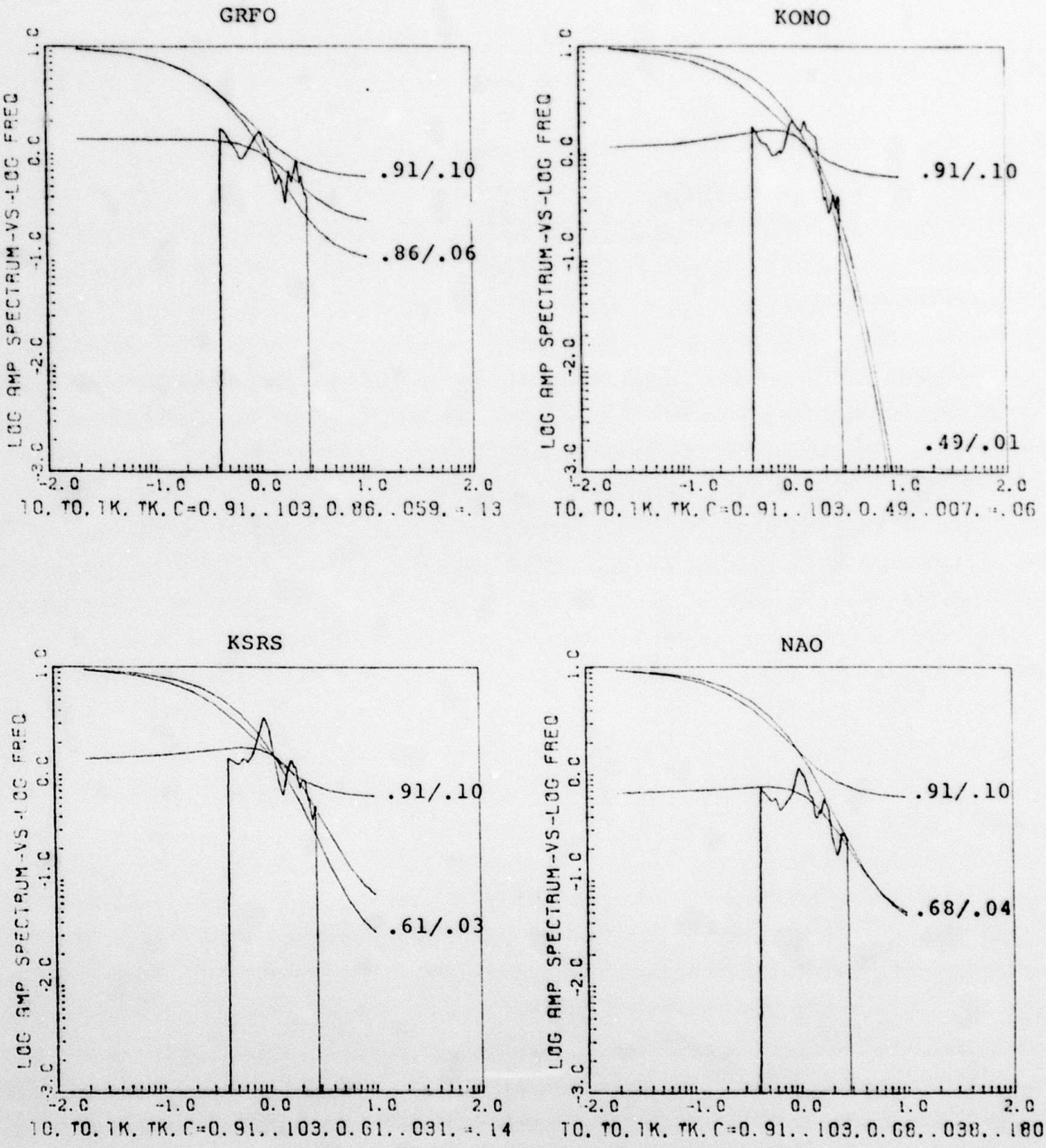

Figure 17. t* inversion on four receiver function spectral ratios using reference station BOCO for NTS sources.

In order to equalize the importance of each model parameter, the weights should be adjusted such that the eigenvalues of equations 14-16 are of equal size. Because t^*_m is on the order of 1.0 sec and τ_2 is on the order of 0.1 sec, weights were set at 0.1 and 1.0, respectively, where layer weights reduce the freedom of the variable. Of course, the weights may be fine-tuned once appropriate starting values have been determined.

With the weights set, the behavior as a function of starting model may be tested. Table 3 shows the result of trying four different starting models for which the t^* and τ_2 trade off to give roughly equivalent path attenuation. The tradeoff between t^* and τ_2 at each station is evident in the table, but the δt^* and $\delta\tau_2$ are consistent independent of starting values. The path from Kazakh to Thailand (CHTO) consistently gives t^*_m on the order of .25 sec and very small τ_2. In the only conflicting result, the squared error increases by 35%. The δt^* between the reference station, ASA, and ANMO is consistently greater than .85, indicating a path with high attenuation. Of the other paths, those to KSRS and PINEDALE show slightly higher attenuation than that to ASA, independent of starting model.

Table 4 shows a test based upon stations in the array for the NTS receiver function spectral ratios. In these tests, the constraints on the inverse are changed by including different data in each run; so the consistency demonstrated in the table is very important. The most

TABLE 3. t^* Inversion on Receiver Function Spectral Ratios Variation with Parameter Starting Values

Starting Value	ALICE SPRINGS		ANMO		CHTO		KSRS		PINEDALE		ERROR
	t^*	τ_2	t^*	τ_2	t^*	τ_2	t^*	τ_2	t^*	τ_2	
$t^* = .45$ $\tau_2 = .05$	.32	.06	1.17	.07	.22	.00	.36	.05	.39	.05	29.1
$t^* = .60$ $\tau_2 = .08$	.46	.09	1.41	.09	.24	.01	.52	.08	.55	.07	28.8
$t^* = .80$ $\tau_2 = .12$	.68	.12	1.64	.11	.28	.02	.75	.12	.76	.10	30.8
$t^* = 1.00$ $\tau_2 = .15$	.83	.17	1.77	.13	.69	.09	.91	.16	.95	.13	42.7

TABLE 4. t^* Inversion on Receiver Function Spectral Ratios

Variation with Stations in Array

BOCO		GRFO		KONO		KSRS		MAJO		NAO		ERROR
t^*	τ_2	t^*	τ_2	t^*	τ_2	t^*	τ_2	t^*	τ_2	t^*	τ_2	
.91	.11	.80	.06	.57	.02	.64	.04	.57	.04			9.2
.94	.10	.88	.06	.51	.01			.52	.03	.69	.04	8.2
1.08	.10	1.08	.07			.56	.02	.38	.00	.63	.03	6.9
1.16	.09			.57	.00	.71	.03	.55	.02	.78	.03	8.0
.91	.10	.86	.06	.49	.01	.61	.03			.68	.04	8.9

significant change is caused by removing station KONO, but examination of Figure 17 shows that KONO ratio has more character than the others. Thus it provides the strongest constraint on the inversion.

Changing the reference station changes only one path in the inverse, but it changes the noise properties of all of the ratios. This in turn changes the tradeoff properties of the inversion, as is demonstrated by Figure 18. In spite of the radical change in reference path properties, however, the same relative secondary path properties are still found by the inversion. Table 5 shows the δt^* between the secondary stations for both inversion runs, and the patterns are nearly exact.

The final test is of the model definition itself. Examination of equation (3) shows that, in the limit as τ_2 goes to zero, the inverse tangent reaches its maximum and $t^*(\omega) = t^*_m$. This is the commonly used constant Q assumption. Another common assumption is that $t^*_m = 1.0$ sec at low frequencies (Lundquist, et al., 1980). In that case, the frequency dependence of t^* is defined entirely by τ_2. Both of these assumptions reduce the number of model parameters, thus reducing the ability of the inversion to fit the data. If the quality of the fit is significantly worse, then the assumption of frequency dependent t^* is justified.

Figures 19-22 show the parameter reduction tests for the two arrays, and comparison should be made to Figures 16 and 17 which show equivalent runs for $t^*(f)$. The results

TABLE 5. Inversion Results and δt^* with Changing Reference Station

	BOCO Reference			ZOBO Reference		
	t^*	τ_2	δt^*	t^*	τ_2	δt^*
GRFO	.86	.06		1.09	.10	
			.37			.32
KONO	.49	.01		.77	.06	
			-.12			-.11
KSRS	.61	.03		.88	.08	
			-.07			-.06
NAO	.68	.04		.94	.08	
			-.18			-.15
GRFO	.86	.06		1.09	.10	

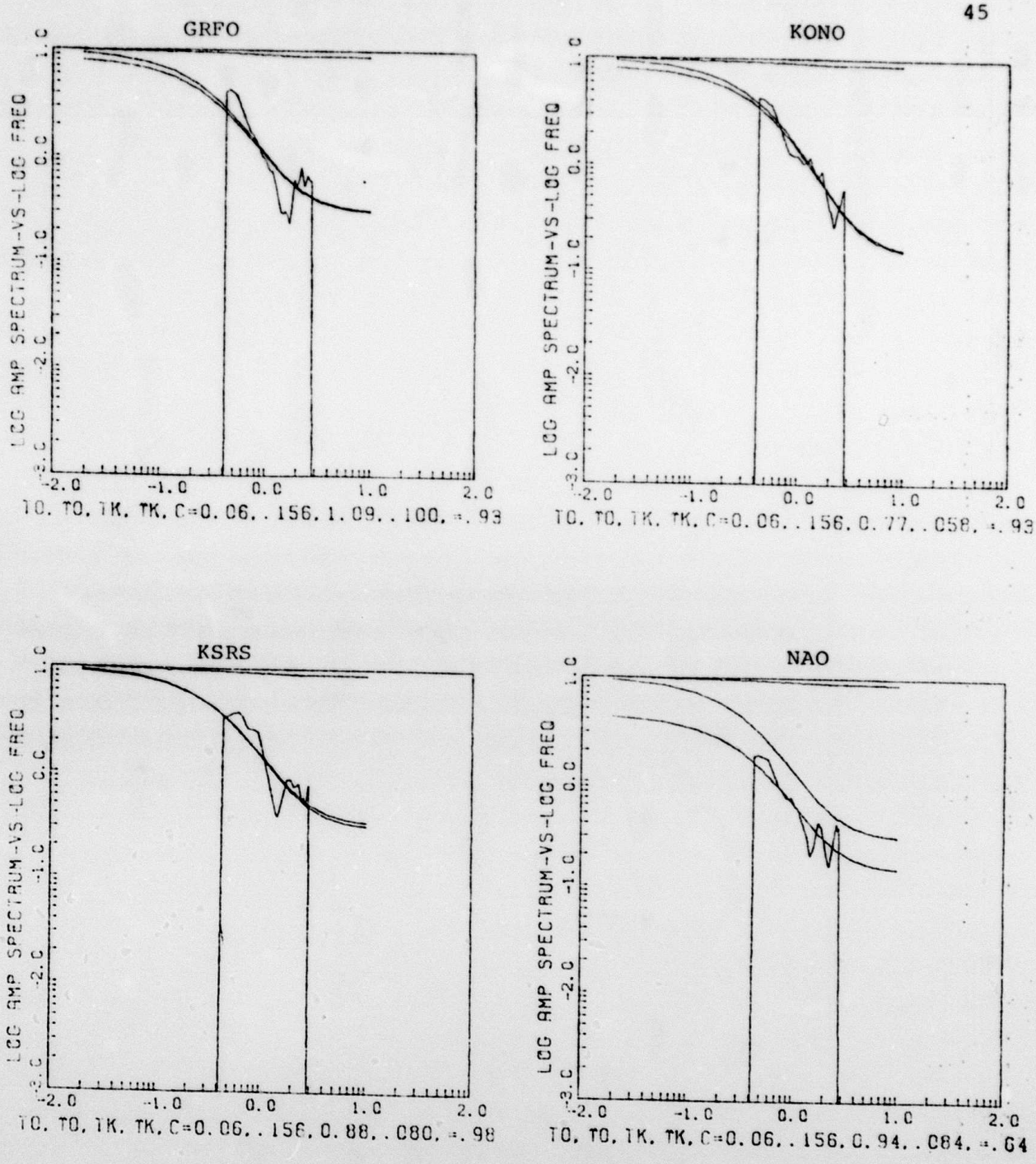

Figure 18. t* inversion on four receiver function spectral ratios using reference station ZOBO for NTS sources. Compare these results with the results from the previous figure.

are summarized in Table 6 which shows t^*, τ_2 and the squared error. The most apparent feature of Table 6 is that the different assumptions do not produce compatible results in common parameters. CHTO and KONO have significantly smaller t^* than the other stations (paths) in their respective arrays when $t^* = t^*(f)$. But when $t^* = t^*_m$, each has a large t^* relative to the other stations. That is, conclusions based upon a frequency independent Q are in direct conflict with results based upon frequency dependent Q. Similar statements may be made about τ_2 under the assumption $t^*_m = 1.0$.

The question still remains as to which assumption is more correct. Based upon the squared error, the $t^*(f)$ assumption is best, but that model has extra parameters with which to fit the data. The difference in errors for the NTS array is not significant, but the difference for the Eastern Kazakh array definitely is. Once again, paths with unusual attenuation provide character in the spectral ratio which can resolve the choice of models. Comparison of Figures 16 and 19 shows that the constant t^* assumption fails to fit the ratios at CHTO and ANMO. Within the resolution of the method, the constant t^* assumption is not an adequate model of path attenuation.

The definitive answer must wait, however, for accurate instrument gains and/or broadband spectral ratios. The three tests for ANMO (Figures 16, 19, 21), for instance, differ greatly at the low frequency end, so the addition of

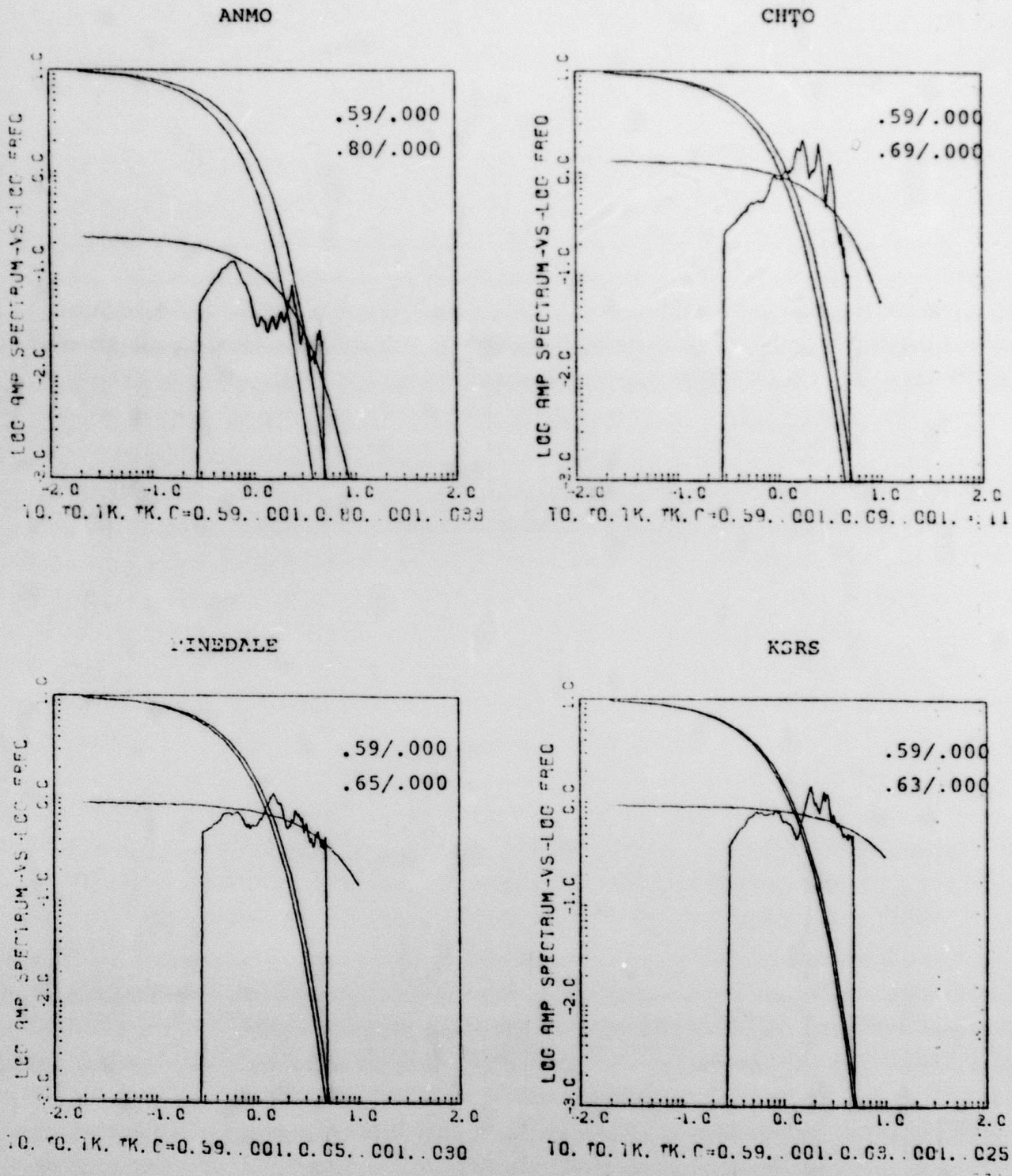

Figure 19. t* inversion on receiver function spectral ratios using frequency independent Q for reference station ASA for Eastern Kazakh sources.

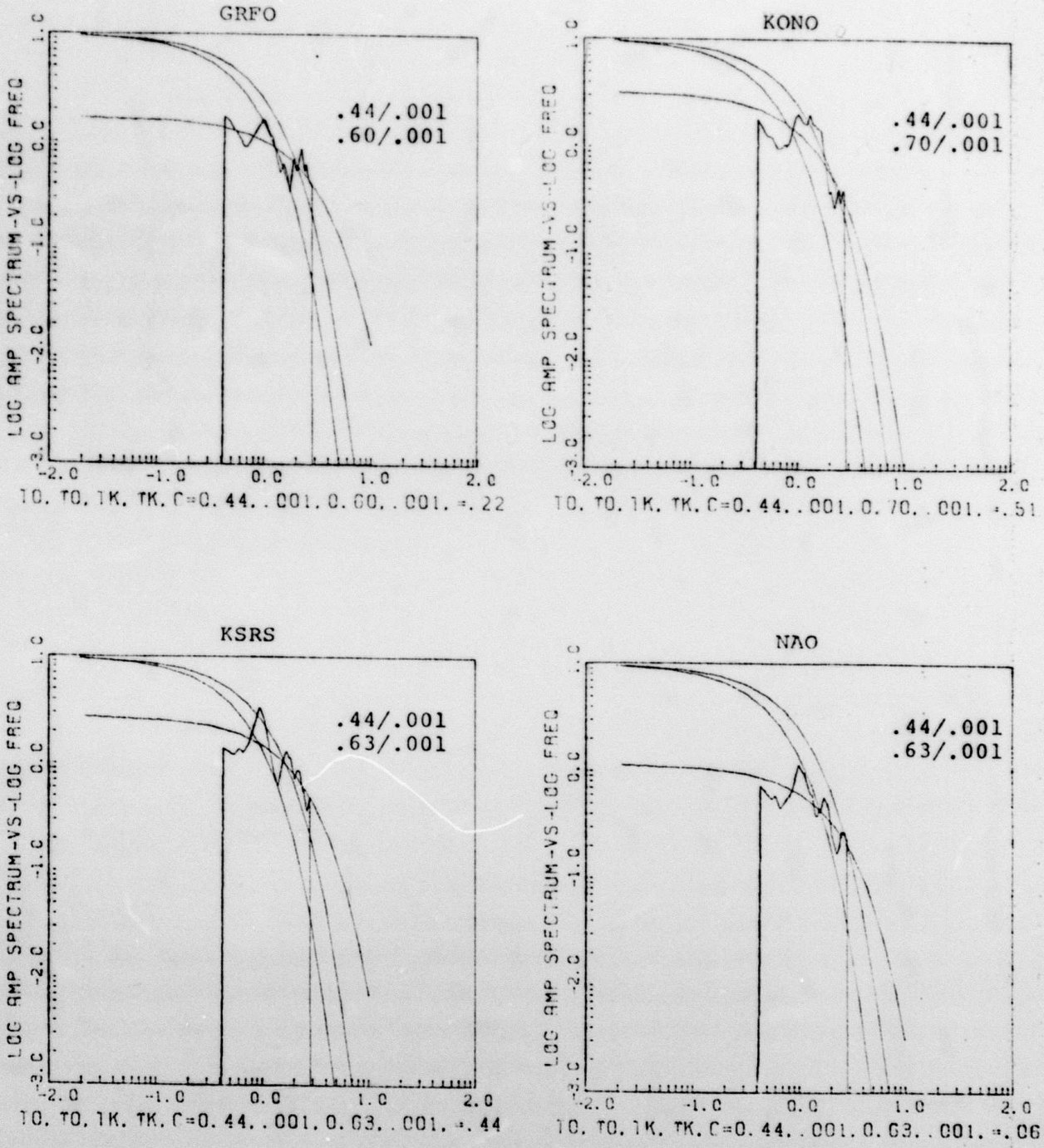

Figure 20, t* inversion on receiver function spectral ratios using frequency independent Q for reference station BOCO for NTS sources.

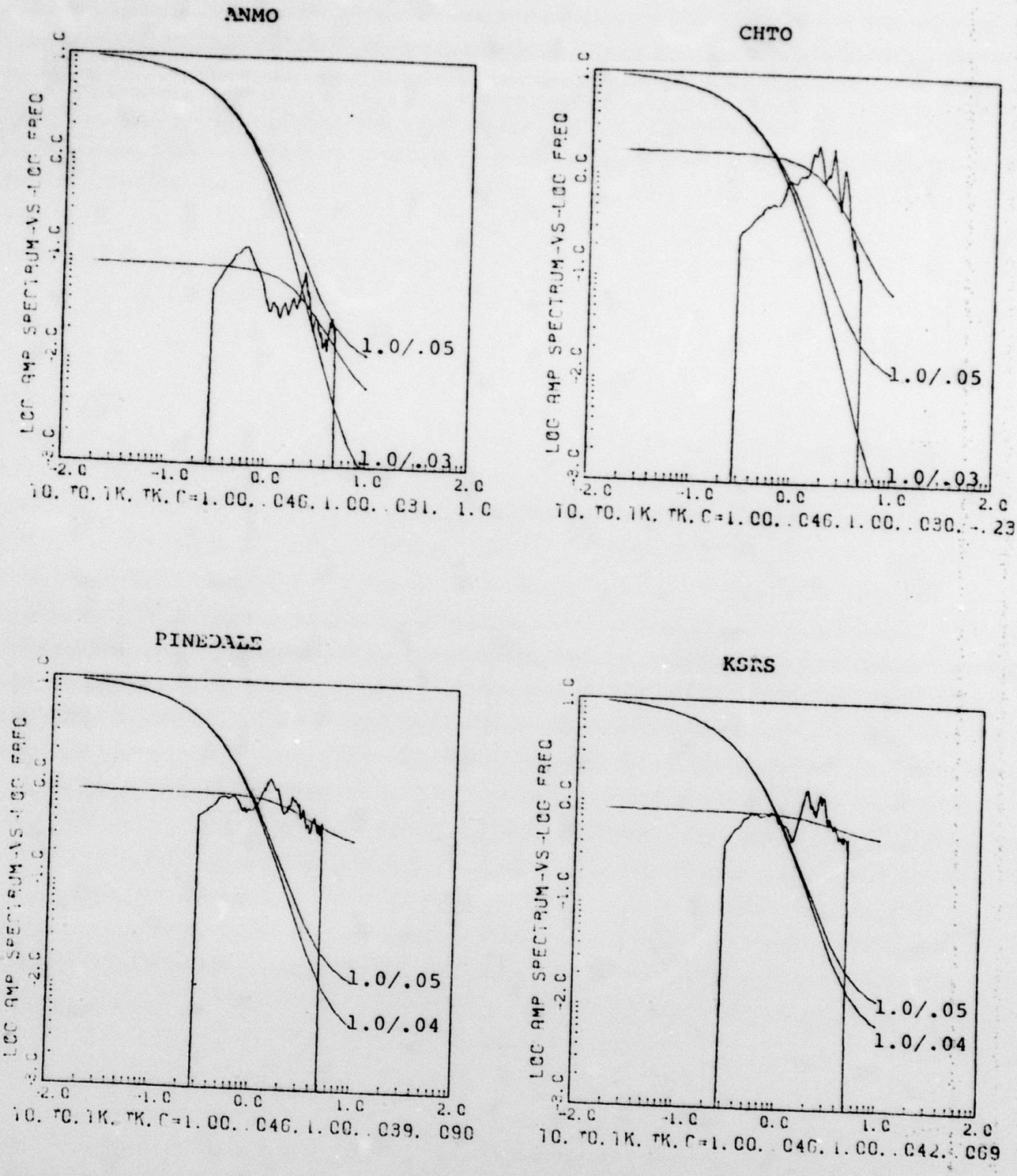

Figure 21. Results of t* inversion on receiver function spectral ratios assuming t*=1. for reference station ASA for Eastern Kazakh sources.

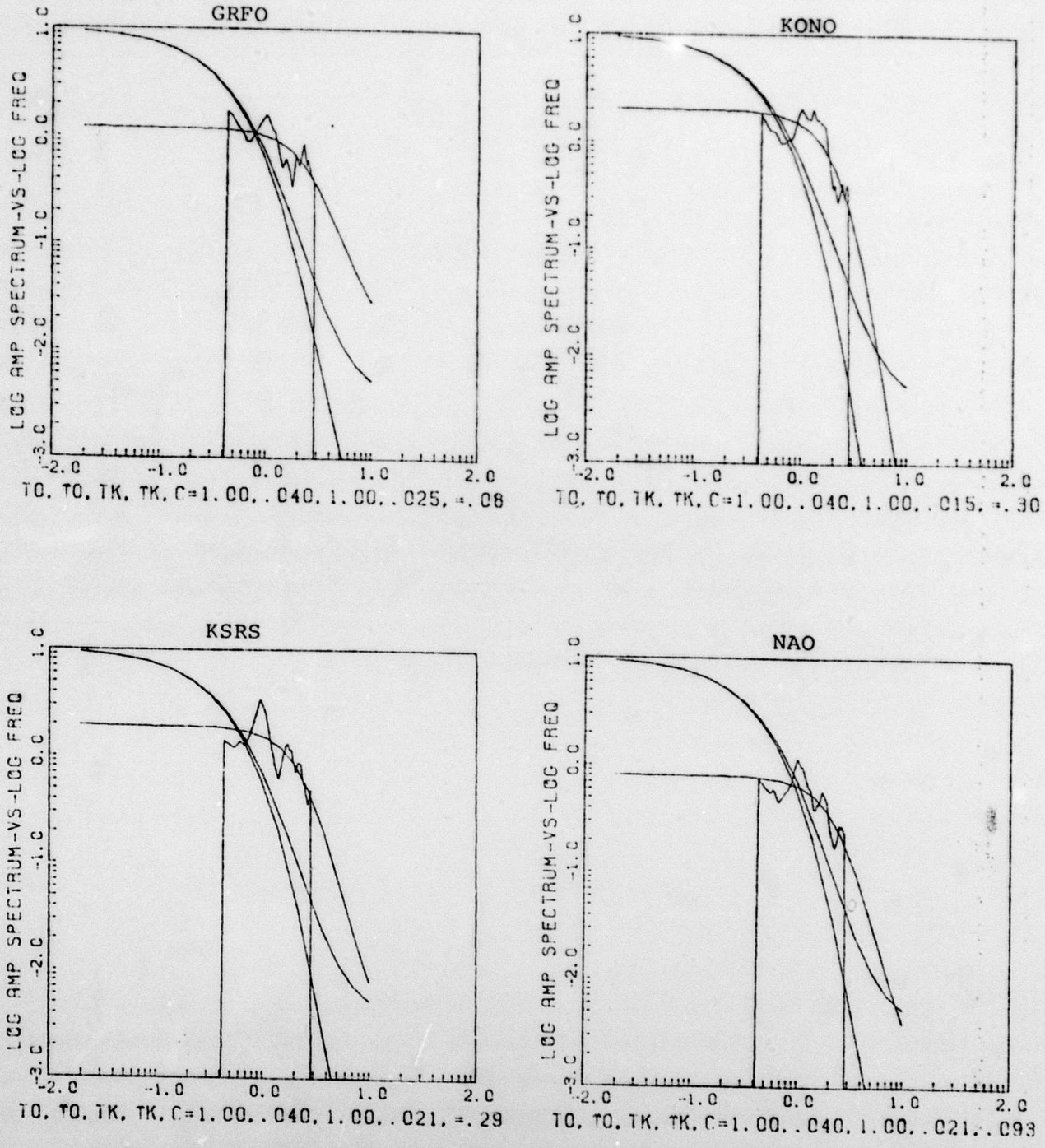

Figure 22. Results of t* inversion on receiver function spectral ratios assuming t*=1. for reference station BOCO for NTS sources.

TABLE 6. Inversion Results and Squared Error Variation with Model Definition

	$t^*=t^*(f)$		$t^*=t^*_m$		$t^*_m=1.0$	
	t^*	ι_2	t^*	ι_2	t^*	ι_2
ASA	.61	.12	.59	.001	1.0	.05
ANMO	1.67	.11	.80	.001	1.0	.03
CHTO	.20	.00	.69	.001	1.0	.03
KSRS	.55	.09	.63	.001	1.0	.04
Pinedale	.70	.09	.65	.001	1.0	.04
ERROR	28.0		41.4		32.4	
BOCO	.91	.10	.44	.001	1.0	.04
GRFO	.86	.06	.60	.001	1.0	.02
KONO	.49	.01	.70	.001	1.0	.03
KSRS	.61	.03	.63	.001	1.0	.02
NAO	.68	.04	.63	.001	1.0	.02
ERROR	8.9		10.5		9.5	

long period contraints can resolve the choice of models. If the relative gains shown here are correct, then the ratio should go through unity at low frequency. In that case, a curve with two inflections is required to fit the ANMO spectral ratios, and neither of the other assumptions is adequate.

IV. CONCLUSIONS AND RECOMMENDATIONS

Both PP/P and receiver function spectral ratios have been interpreted in terms of $t^*(f)$, and both tests have found that inadequate data sets limit the resolution of model parameters. In each case significant noise within the passband of the ratios was due to crustal transfer functions. Among other conclusions to be made here is the fact that crustal effects are very significant, much more important than might be estimated via a Haskell-Thompson formulation.

Tradeoff problems also limit the accuracy of the inversion technique. t^* and τ_2 may trade off to give roughly equivalent apparent attenuation over any narrow bandwidth, and the parameters for two paths can trade off in a spectral ratio. Thus differences are more correctly estimated than absolute values. The PP/P ratios determine a δt^* which can be associated with the bounce point, and the most reliable result for central Asia gives $t^*=0.8$ sec for the upper mantle beneath the Eastern Kazakh test site.

Receiver function spectral ratios can determine relative path properties for paths from a common source region. Considering paths about the Eastern Kazakh test site, station CHTO sees very little attenuation, and ANMO sees a very high attenuation. The δt^* between these two stations is more than 1.2 sec. Stations KSRS, Pinedale and Alice Springs are intermediate, averaging $\delta t^*=.4$ greater than CHTO. For paths about NTS, ZOBO sees a very low path

attenuation, and KONO has somewhat lower attenuation than KSRS or NAO. The δt^*=.2 sec between KONO and NAO is of interest because of the proximity of the two stations.

It is of interest to note that t^* values found by this inversion technique cluster in the range .4 to 1.0 sec, and τ_2 is never found to be greater than .18 sec. Though this is somewhat dependent upon starting models, it is clear that t^* values do not tend toward values greater than 1.0.

Perhaps the most important conclusion sought by this research is a definitive statement as to the frequency dependence of Q. Within the limitations of the data sets and the method, it appears that the assumption of constant Q (or constant t^*) does not provide an adequate fit to the data sets. An unequivocal conclusion, however, will require more work, data sets with greater bandwidth, and accurate instrument calibrations.

V. REFERENCES

Gurevich, G.I., A basic feature of the propagation and attenuation of seismic vibrations, in Aspects of the Dynamic Theory of Seismic Wave Progagation Collection, V. 7, Sbornik, 1964.

Jackson, D.D., and D.L. Anderson, Physical mechanisms of seismic wave attenuation, Rev. Geophys. Space Phys., 8, 1-63, 1970.

Lieu, H.P., D.L. Anderson, and H. Kanamori, Velocity dispersion due to anelasticity; implications for seismology and mantle composition, Geophys. J. Roy. Soc., 47, 41-58, 1976.

Lundquist, G.M., The frequency dependence of Q, Ph.D. thesis, Univ. of Colo., Boulder, 1979.

Lundquist, G.M., G.R. Mellman and D.M. Hadley, Relative receiver functions for three different array concepts, SGI-R-80-021, Sierra Geophysics, Inc., Redmond, Wash., 1980a.

Lundquist, G.M., G.R. Mellman and D.M. Hadley, Relative receiver functions, SGI-R-026, Sierra Geophysics, Inc. Redmond, Wash., 1980b.

Lundquist, G.M., G.R. Mellman and D.M. Hadley, Relative receiver functions for the eastern Kazakh global array, SGI-R-80-030, Sierra Geophysics, Inc., Redmond, Wash., 1980c (classified report).

Lundquist, G.M., M.N.S. Kam, G.R. Mellman and D.M. Hadley, Relative Receiver Functions for the NTS Global Array, SGI-R-81-042, Sierra Geophysics, Inc., Redmond, Wash., 1981 (classified report).

Lundquist, G.M. and V.C. Cormier, Constraints on the absorption band model of Q, J. Geophys. Res., 85, p. 5244, 1980.